Aus dem Institut für
Laboratoriumsmedizin, Klinische Chemie und Pathobiochemie
der Medizinischen Fakultät Charité – Universitätsmedizin Berlin

DISSERTATION

Microvillus Positioning of L-selectin and CD44 and its Impact on Leukocyte Adhesion

zur Erlangung des akademischen Grades
Doctor medicinae (Dr. med.)

vorgelegt der Medizinischen Fakultät
Charité – Universitätsmedizin Berlin

von

Konrad-Robert Buscher
aus Freiburg i.B.

Gutachter 1. Prof. Dr. R. Tauber

2. Prof. Dr. P. Knaus

3. Prof. Dr. D. Vestweber

Datum der Promotion: 07.09.2012

Contents

Die praktischen Arbeiten wurden durchgeführt im

- Institut für Laboratoriumsmedizin, Klinische Chemie und Pathobiochemie
  Charité – Universitätsmedizin Berlin
  Arbeitsgruppe: Univ.-Prof. Dr. R. Tauber, Dr. J. Dernedde
- Division for Inflammation Biology
  La Jolla Institute for Allergy and Immunology, California, USA
  Principal Investigator: Klaus Ley, M.D.

1 Introduction

1.1 The Microcirculation

The terminal branches of the circulation are represented by a spacious microvascular network that ranges from first-order arterioles to first-order venules. A microvascular subunit ideally consists of a single arteriole and venule between which extends an extensive network of capillaries and in some tissues a metarteriole providing a well regulated shortcut. Terminal arteries become as small as 25 µm and merge then into arterioles. Both share a common histological structure of an inner layer of endothelium, an internal elastic lamina and a single or multiple layers of innervated vascular smooth muscle cells in arterioles or arteries, respectively. Reflecting their functional needs, capillaries lack the relatively thick muscle layer. Instead, a single layer of 200-300 nm thin endothelial cells surrounded by a basement membrane is loosely embedded in a fine network of reticular collagen fibers (1).

The primary function of the circulation is to maintain a suitable environment for the tissues according to need. Arterioles mainly serve the needs of regulating blood pressure, body temperature and blood distribution. They are capable of large changes in vessel diameters and may dilate up to 50% of their normal state or contract leading to complete obstruction. With the 4^{th} power relation between radius and flow as described by Poiseuille and Hagen in 1830 (Equation 1), the enormous impact on vascular resistance becomes apparent. Because the inner radius of capillaries is about 4 times smaller than arterioles, the individual resistance of capillaries is much higher but considering the about 10^3 times higher number of units, the total vascular resistance is only about 1/5. Therefore, arterioles account for 50-60% of the resistance in muscle tissue while capillaries only for about 15%. The capillary bed is the principal site for blood tissue exchange processes. Gas, water, nutrient and waste product exchanges fulfill nutritional purposes. Only 10% of the total vascular resistance is determined by postcapillary venules. These, however, have an important influence on the hydrostatic capillary pressure and thus on fluid exchange (2).

The endothelial monolayer lining the entire circulatory system is a main effector site of the immune response and homeostasis of multicellular organisms. Due to its privileged situation at the interface between blood and tissue, the endothelium is affected by both luminal and abluminal signals. As a result, the genetic expression pattern is highly dynamic and reflects constant changes in blood composition, mechanical forces and disruption of the homeostasis such as injury, infection or disease. A well balanced pattern of adhesion receptors expressed on the endothelial cell layer allows the communication to freely flowing cells which in turn can be activated to exit the bloodstream (3). This sequential process is summarized in chapter 1.2.1. Apart from important roles in physiological situations, the endothelium also takes centre stage in a variety of pathological conditions (chapter 1.1.2).

1.1.1 Hemodynamics

Given the corpuscular suspension of blood as well as the pulsatile blood flow, flow turbulences at bifurcations and endothelial defects, massive variation of vessel diameters and shear stress, biophysical aspects are complex yet essential for understanding microvascular function.

Viscosity and Hematocrit

The viscosity of blood is strongly dependent on the hematocrit and tube diameter. Erythrocytes with a volume fraction of about 45% in human adults exert a large influence on flow properties in microvessels. Lateral migration of erythrocytes towards the longitudinal center of the tube along the parabolic velocity profile (Hagen-Poiseuille’s law, Equation 1) causes changes of the hematocrit within the tube compared to the hematocrit in a static environment. This is known as the Fåhraeus effect (4,5). Importantly, it implicates a cell-depleted layer adjacent to the endothelial wall. The relationship with the tube diameter was first shown by Fåhraeus and Lindqvist (6). Diameters below 300 µm provoke a significant decline of the apparent hematocrit with a minimum at 5-7 µm.

$$Q = \frac{\pi}{8} * \frac{r^4}{l} * \frac{1}{\eta} * \Delta P$$

Equation 1: Hagen–Poiseuille law describing the flow (Q) in a cylindrical tube as a function of the radius (r), the length (l), the viscosity (η) and the pressure difference (∆P).

Diverging bifurcations lead to an unproportional separation of plasma and cells causing a decreased hematocrit in daughter vessels (7). One reason is the cell-free layer close to the vessel wall. This phenomenon is referred to as “plasma skimming”. Another reason is the increasing importance of the erythrocytes’ size as the diameter of the diverging vessel decreases which is called “red cell screening”. As a consequence, the vascular hematocrit is not equal at all identical segmental levels of the capillary network but varies all over the microvascular bed as a function of topological geometry and cellular properties. Erythrocytes feature a mean diameter of 8 µm whereas microvessels become as small as a few micrometers. Length and connectivity of segments also vary widely. In conclusion, hemodynamics in the microcirculation are very heterogeneous and reflect the importance of regulating blood distribution in accordance to need.

Affect on Leukocyte Adhesion

Although being much less concentrated, white blood cells (WBCs) also play an important role in biophysical models of blood flow as they increase blood flow resistance (8). Moreover, their biological activity is crucially affected by the microvascular environment. The Fåhraeus effect and high shear stress draw flowing leukocytes away from the vascular wall and challenge the appropriate reaction to endothelial signals. These physical forces become more accentuated as venules get increasingly wider.

When WBCs enter small branches of the microcirculation, the spherical cell shape and larger cell volume affect a slower movement and lead to an accumulation of erythrocytes upstream and an erythrocyte-depleted area downstream of the WBC. After the passage to a wider postcapillary section, piled up erythrocytes now can pass and thereby cause flow disturbances that displace the WBCs towards the endothelial layer (9). Therefore, leukocyte rolling predominantly takes place at postcapillary segments with low-shear profiles.

Local vessel dilation upon endothelial activation might also facilitate this process. Cell-side adaptation to these hemodynamics includes the formation of surface protrusions (chapter 1.3.1).

1.1.2 Role in Inflammation

The complex response to injury in order to protect and maintain the homeostasis of the organism is called inflammation (derived from "*inflammatio"*, Latin). It enables the body to sufficiently encounter harmful stimuli such as physical injury, infection, chemical irritants, ionizing radiation or immune reactions as a protective attempt to remove the threat and restore the integrity of the tissue.

Acute inflammation is clinically characterized by rubor, calor, dolor, tumor (first noted in *De Medicina* by Aulus Cornelius Celsus, ~ *25 BC †50 AD) and functio laesa (added by Galen of Pergamon, ~ *129 †199 AD). This early description already reflects the molecular adaptation of the microcirculation upon inflammation (3). Various vasodilators such as nitric oxide, adenosine and prostacyclin are released, noticeable as redness (rubor) and heat (calor). The exudation of plasma proteins is a result of the increased permeability of the vascular endothelium and the basal membrane causing a tissue swelling (tumor) through a decreased osmotic (colloid) gradient. As diabetic neuropathy and syringomyelia point out, the loss of pain perception can result in severe injury or delay tissue regeneration. Therefore, stimulation of nociceptors causing pain (dolor) constitutes an important evolutionary factor to preserve the integrity of an organism.

The main purpose of vasodilatation is the increase in blood flow which provides enhanced accessibility of immune cells to the site of inflammation. In the acute phase, the innate immune system takes action and identifies pathogens through pathogen-associated molecular patterns (PAMPs) interacting with pattern recognition receptors (e.g. Toll-like receptors, C-type lectins, scavenger receptors) and antibody opsonization. Neutrophil granulocytes and natural killer cells are necessary for early phagocytosis and killing of microbes. Mononuclear phagocytes such as macrophages and dendritic cells ignite the adoptive immunity via antigen presentation to lymphocytes in secondary tissue and support

inflammation by secreting cytokines. In response to the secreted inflammatory mediators, mainly interleukin 1 (IL-1) and tumor necrosis factor (TNF), the endothelial cell layer adopts a distinct gene expression pattern leading to presentation of specialized adhesion molecules on the lumen-faced site of the cells. This provides the required platform for cellular communication. Among the variety of reactions, the interaction between blood effector cells and the activated endothelium triggering cell transmigration is seen as a key step that crucially affects the efficiency of the immune response.

A variety of pathologies emphasize the importance of a close regulation as both the lack (leukemia, AIDS, iatrogenic immune suppression) and the overstimulation (rheumatoid arthritis, lupus erythematosus, inflammatory bowel diseases) of inflammation severely compromise the organism (10-12). Endothelial dysfunction is a hallmark for vascular and inflammatory diseases including arthrosclerosis (10,11,13) and diabetes mellitus (14-16).

1.2 Cell Adhesion in the Immune System

1.2.1 Leukocyte Adhesion Cascade

Historical background

After William Harvey had postulated a closed systemic circulation in the 17th century and van Leeuwenhoek had developed the first microscope with sufficient resolution to see single erythrocytes in the 18th century, the ground was laid to further investigate microcirculation. In the 19th century, the first description of leukocyte rolling comes from Rudolf Wagner (17) which was later confirmed by Rudolf Virchow (18) (Figure 1.1). Elie Metchnikoff added a detailed phenotypic description of the underlying adhesion cascade and defined different types of leukocytes (19) for which he was awarded the Nobel Prize in 1908. These groundbreaking works introduced the principal concepts of inflammation, leukocyte adhesion and endothelial activation, all of which frame our current understanding of immunity.

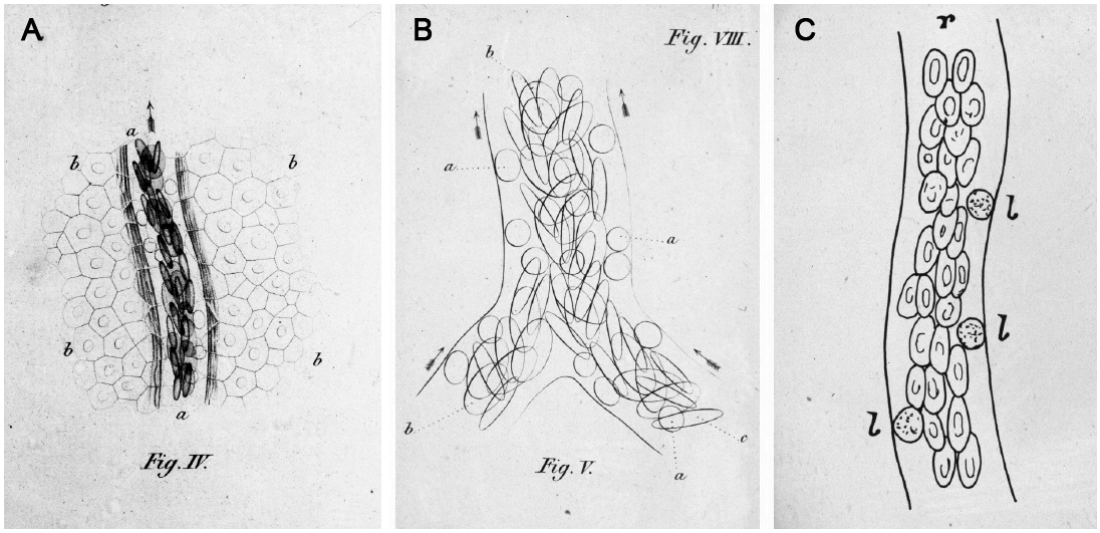

Figure 1.1: Intravital microscopy observations of the microcirculation and leukocyte rolling from (A) (B) Rudolf Wagner **(17)** and (C) Rudolf Virchow **(18)** in the 19th century.

Adhesion as a Multistep Process

Neutrophil invasion at sites of inflammation as well as lymphocyte recirculation from blood into secondary lymphoid tissue require that free-flowing leukocytes become activated after antigen encounter and subsequently exit the blood stream. At the molecular level, the cells undergo a closely orchestrated cascade of interactions with the endothelium, each step consisting of a characteristic pattern of receptors, their ligands, cytokines and chemoattractants (20,21).

Chemokine-activated G-coupled receptors ignite leukocyte activation with subsequent changes in receptor composition and cell morphology. While selectins initiate the very first contact to the endothelium (22), $\alpha_4\beta_1$-integrins (23,24), β_1-integrin very late antigen 4 (VLA-4) (25), β_2-integrins lymphocyte function-associated antigen 1 (LFA-1) and macrophage 1 antigen (MAC-1) (23,26) further decelerate the rolling leukocyte. Complete arrest is induced by the intercellular adhesion molecule 1 (ICAM-1) and vascular cell adhesion molecule 1 (VCAM-1) (27,28) expressed on the endothelial layer and succeeded by trans- or paracellular extravasation (Figure 1.2).

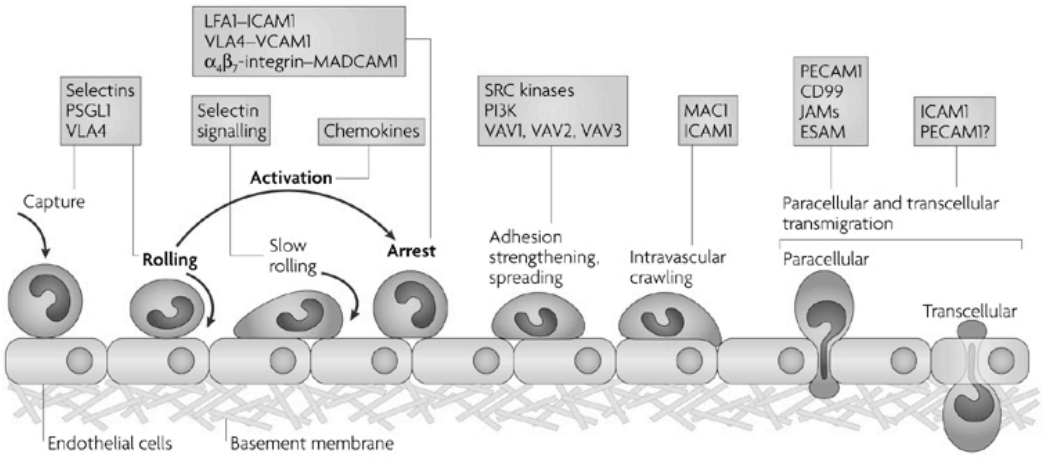

Figure 1.2 Leukocyte adhesion cascade divided into six different steps leading to the cellular extravasation to inflamed tissue. Most communication between leukocytes and the endothelium takes place in the postcapillary section. Selectins initiate the first contact to endothelial cells (capturing) and upon cytokine-triggered activation rolling and slow rolling under conditions of blood flow. Further steps are mainly affected by integrin and immunoglobulin gene families. Figure from **(21)**.

1.2.2 Selectins

Selectins are a carbohydrate binding family of three C-type lectins termed according to their localization L-, E-, P-selectin (L for leukocyte, E for endothelium, P for platelets). They mediate leukocyte adhesion under flow and are exclusively expressed by bone-marrow-derived and endothelial cells (Table 1.1). Being involved in chronic and acute inflammation processes, including post-ischemic inflammation in muscle, kidney and heart as well as skin inflammation, atherosclerosis, glomerulonephritis and lupus erythematosus, selectins and their receptors represent an important target for pharmaceutical intervention in a variety of human diseases (29).

Table 1.1 Selectin expression patterns. Adapted from **(32)**.

Selectin	Cell/tissue	Expression pattern
L-selectin	Myeloid cells	Constitutive
	Naive T cells	Constitutive
E-selectin	Skin endothelium	Constitutive
	Inflamed endothelium	Inducible
P-selectin	Platelets	After activation
	Lung endothelium	Constitutive
	Choroid plexus	Constitutive
	Peritoneal macrophages	Constitutive

P- and E-selectin expression is partly inducible upon activation while L-selectin is constitutively expressed on myeloid and native T cells (Table 1.1). Weibel-Palade bodies in endothelial cells and α-granules in thrombocytes store P-selectin which can be quickly liberated app. 10 min after activation by fusing with the cell membrane (30). In contrast, endothelial E-selectin is transcriptionally regulated and requires some hours to be fully functional presented on the lumen-sided cell surface (31). Leukocyte selectin shows a constitutive expression pattern and is regulated by protease-controlled ectodomain shedding following cellular activation (see following chapter). These differences in selectin-expression are thought to precisely regulate the sequential process of the adhesion cascade.

L-selectin

The adhesion receptor L-selectin (CD62L, former synonyms: LAM-1, MEL-14 antigen, Leu-8, MECAM-1) is a bitopic type I integral membrane protein binding defined carbohydrates on select glycoproteins. It consists of a lectin domain responsible for ligand binding, an epidermal growth factor (EGF) domain, two short consensus repeats (SCR), a membrane-spanning region, and a short 17-amino acid cytoplasmic tail (Figure 1.3) (33,34). The receptor also harbours a membrane-proximal cleavage site that is proteolyzed after leukocyte activation (35) and leads to soluble L-selectin (sL) in the bloodstream. L-selectin as other selectins too, possesses multiple N-glycosylation sites (34,36). In humans, the level of L-selectin glycosylation depends on the cell type. Western Blot data reveal a specific molecular mass of 74 kDa in neutrophils but ~105 kDa in lymphocytes (37,38).

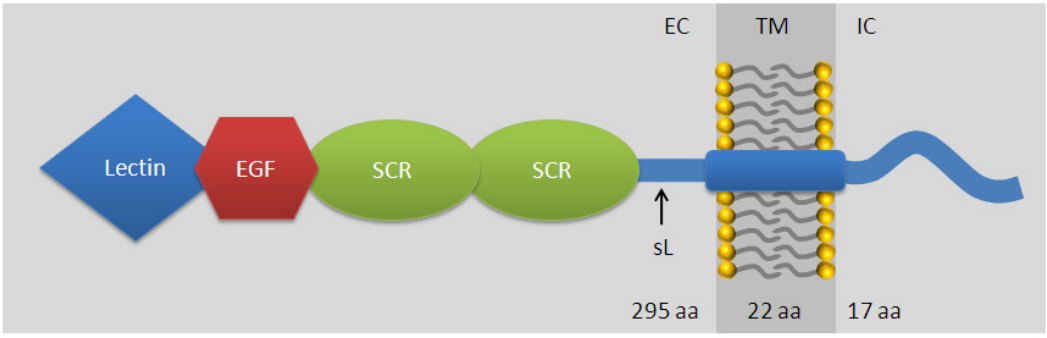

Figure 1.3 Schematic structure of the transmembrane receptor L-selectin. The lectin domain is located at the N-terminal end and is responsible for ligand binding. In contrast to E- and P-selectin, it only consists of two SCR domains. sL indicates the cleaving site of the extracellular domain upon leukocyte activation. aa = number of amino acids. EC = extracellular, TM = transmembrane, IC = intracellular.

All subsets of neutrophils, monocytes and lymphocytes constitutively express L-selectin (39), predominantly on the tips of thin membrane protrusions (chapter 1.3). Leukocyte tethering and rolling on inflamed endothelium (22) and lymphocyte homing to secondary lymphoid tissue *in vivo* (40) is crucially dependent on L-selectin but requires a threshold hydrodynamic shear. When flow is stopped, rolling cells detach (41,42). The increasing dislodging fluid shear strengthens each selectin-ligand complex, prolonging its lifetime and thus stabilizing leukocyte rolling. The explanation for this phenomenon was found in the molecular bond kinetics using atomic force microscopy (43) and is called *catch bond* (44) in contrast to bond-weakening *slip bonds*. On an atomic level, a hinge region between the lectin- and EGF-domain allows an allosteric flexibility regulating mechanical properties of selectin bonds (45).

In an effort to better understand the orchestrated deployment of selectins and the ability to activate integrins, their respective counterreceptors were studied extensively. The tetrasaccharide sialyl Lewisx (sLex) turned out to be the natural binding epitope common to all three selectins. This minimal ligand is the reason why P-selectin glycoprotein ligand 1 (PSGL-1) shows binding to E-, P- and L-selectin. It is found on inflamed endothelium and binds them in a calcium dependent manner through sLex on O-linked glycans and, for high affinity L- and P-selectin binding, adjacent sulfated tyrosine residues (46,47). L-selectin dependent lymphocyte migration to secondary lymphatic tissue requires ligands on high endothelial venules (HEVs) subsumed as peripheral node addressins (PNAd). Most of these ligands are defined by MECA-79 monoclonal antibody (mAb) binding. Known components are CD34 (48), glycosylation-dependent cell adhesion molecule 1 (GlyCAM-1) (49), Podocalyxin (50) and Endomucin (51) all of which belong to the family of sialomucins. Selectin-mediated lymphocyte rolling in mesenteric lymph nodes is dependent on mucosal addressin cell adhesion molecule 1 (MAdCAM-1) (52). Another ligand with yet undefined physiological relevance is Nucleolin (53).

Several *in vivo* data emphasize the importance of L-selectin for the homeostasis of the immune system. Activated and adherent cells can multiply the cellular response by engaging in L-selectin-PSGL-1 interactions with passing leukocytes

(secondary tethering) *in vivo* (54-56). Neutrophil extravasation can be significantly reduced by blocking L-selectin with mAbs (57). Knock-out mice show a profound defect of lymphocyte accumulation in secondary lymphatic tissue and of neutrophils at sites of inflammation (58). Jung and Ley differentiated the individual contributions of E-, P- and L-selectin using gene-targeted mice (59).

1.2.3 CD44

CD44 is a family of surface-expressed glycoproteins involved in cell-cell- and cell-matrix-interaction (60). The observation of upregulated CD44 expression in most neoplasias led to an increased scientific interest (61).

With 20 exons given, it comprises more than 17 isoforms formed by alternative mRNA splicing. Additional posttranslational modification allows many varied functions. Due to its high versatility, CD44 is almost ubiquitously expressed on most tissues including bone marrow stromal cells. Hyaluronic acid (HA) was found to be the main physiologic ligand (62) but in vivo interactions with osteopontin, collagens and metalloproteinases have also been described. Furthermore, it is a potent ligand for L-selectin and E-selectin as shown by an example of sialofucosylated form called HCELL (63). The intracellular domain of CD44 communicates with the cytoskeleton via ankyrin and the ezrin-moesin-radixin (ERM) family (64).

As regards the immune system, CD44 is mainly involved in lymphocyte activation, adhesion and proliferation (65). While L-selectin-triggered interactions are necessary for cell tethering to the endothelium in peripheral tissues, CD44 takes the lead in lymphatic tissues (66). Homing of hematopoietic stem cells to bone could also be partly attributed to CD44 triggered cell adhesion (67).

1.3 Receptor Surface Segregation

Distinct cell surface receptor segregation is a widely observed phenomenon with effects on cell proliferation, migration and tumorigenesis (68). In contrast to polarized cells featuring an apical and basolateral side physically separated by tight junctions, non-activated blood cells consist of a uniform lipid bilayer.

However, studies about ultrastructural receptor surface localizations of blood cells revealed that certain molecules populate only defined parts of the plasma membrane. This emphasizes the existence of cell surface compartments in non-polarized cells.

1.3.1 Cell Surface of Leukocytes

The complex surface of leukocytes features sheet-like protrusive structures such as lamellipodia and ruffles and finger-like protrusions such as microvilli (MV) and filopodia (69). A lamellipodium resembling a two-dimensional mesh which is capable of propelling a cell across a substrate is often located at the leading edge of motile cells. Filopodia are microspikes extending beyond the leading edge of lamellipodia and are thus also crucial to cell motility (70). Microvilli particularly decorate epithelial layers such as intestinal enterocytes (brush border), inner ear (stereocilia) and proximal kidney tubules. Their actin-dependent architecture and biological role in absorption, secretion and mechanotransduction is well known. While they remain relatively stable with a length up to 2000 nm in epithelia, the dimensions of leukocyte microvilli are much smaller, not polarized and they undergo high dynamic changes in length.

Surface morphology data of leukocytes were previously obtained using transmission electron microscopy (TEM) (39) and scanning electron microscopy (SEM) (71). The two-dimensional character of TEM does not allow distinguishing microvilli from ruffles. Apart from that limitation, both studies are quantitatively consistent. Most of the spherical cell body is covered with membrane protrusions. Microvilli dominate in lymphocytes whereas sheet-like ruffles mostly occur in polymorphonuclear cells (PMNs) and monocytes. The average length of ~300 nm of microvilli and ruffles found in electron microscopy is also supported by mechanical measurements with a micropipette manipulation system (72). Impressions of the surface landscape of human leukocytes are provided in Figure 1.4 and a quantitative analysis in Table 1.2.

Although both epithelial and leukocyte structures rely on tightly regulated assembly and disassembly of actin filaments, the individual dynamics vary immensely (69). Using scanning ion conductance microscopy, the cell membrane

and associated short, nonspecialized microvilli of living cells were visualized and shown to be highly dynamic in several human cell lines (73). With an average lifetime of 12 ± 6 min, each individual plasmatic extension undergoes a constant life cycle. Their ability to aggregate into more stable structures is proposed to be essential for the organization of specialized surface structures such as microvilli found on intestine or kidney cells.

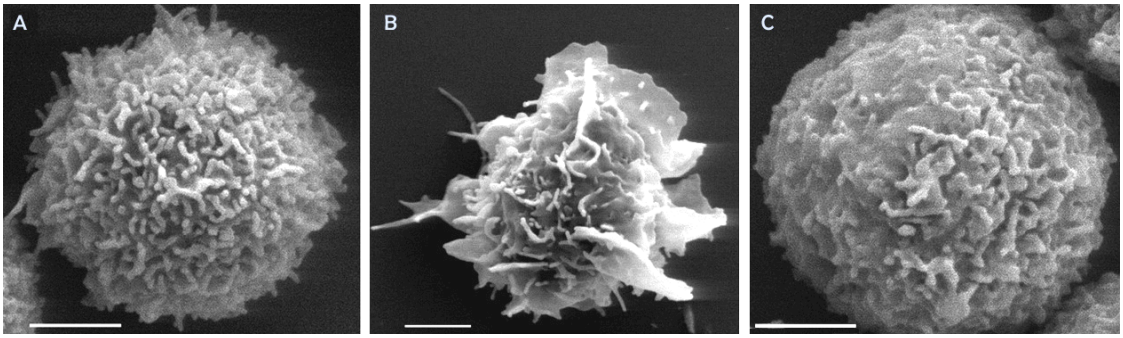

Figure 1.4 Surface morphology of human leukocytes. Scanning electron micrographs of a human (A) lymphocyte, (B) PMN and (C) monocyte. Scale bars represent 2 µm. Figure from Majstoravich et al. **(71)**.

Table 1.2 Surface morphology of human leukocytes. Data presented as mean ± standard deviation. Cell diameter and length of protrusion based on TEM by Bruehl et al. **(39)**. Other data based on SEM by Majstoravich et al. **(71)**. MV = microvilli. PMN = Polymorphonuclear cells. Surface protrusions as % of surface area.

	PMNs	Lymphocytes	Monocytes
Cell Diameter [µm]	8 ± 1	6 ± 1	8 ± 1
Surface Protrusions			
Small ruffles [%]	77	0	0
Large ruffles [%]	20	11	84
MV [%]	0	85	13
Length of Protrusion [nm]	290 ± 170	340 ± 190	390 ± 280
MV density [villi/µm^2]		4.1 ± 1.0	

Parallel bundles spanning the length of microvilli organize the actin filaments and serve as a platform to crosslink a number of proteins. The overlying plasma membrane is intimately associated through these core filaments. Therefore, the microvillus microstructure adopts a specialized molecular composition distinct from other cytoskeletal parts of the cell. In human T-lymphocytes a higher

distribution of e.g. the Arp2/3 complex, actin α and β, Ezrin, Moesin, Radixin and NHERF1 can be found (74). Beyond morphological determinations further details about the structure and dynamics of leukocyte MV are largely unknown.

Leukocyte MV serve as active grouping sites for a variety of surface receptors including L-selectin (75), α_4-integrins (76), PSGL-1 (77,78), CD4 and the chemokine receptors CCR5 and CXCR4 (79). Several tetraspans are also predominantly localized to microvillus protrusions in K562 cells, namely CD53, CD63, CD81 and CD82 (80). In contrast, the hyaluronan receptor CD44 (75) and the integrins $\alpha_M\beta_2$ (MAC-1) and $\alpha_L\beta_2$ (LFA-1) (81,82) show expression on the planar cell body excluding microvilli.

1.3.2 Mechanisms of Protein Segregation to Microvilli

Although leukocyte surface structures, including microvilli, ruffles, filopodia and lamellipodia, are well described (69), a detailed biochemical understanding of their receptor composition is still largely missing. Likewise, very little is known about the sorting and trafficking mechanisms that transport and segregate proteins to the MV or the planar cell body.

To date, it is well recognized that cytoplasmic interactions can regulate protein sorting (83). L-selectin's distribution on microvilli is abolished upon mutation of its intracellular Ezrin/Radixin/Moesin (ERM) binding site (84). The tail-truncated L-selectin mutant LΔcyto only containing the membrane proximal ERM binding site of the IC domain still localizes to microvilli (85). As a consequence, cytoskeletal linkage to ERM is commonly believed to be a main determinant of surface localization. However, CD44 links to ERM proteins, too (64), yet it shows an inverse surface expression pattern only on non-protrusive sections. Hence, definitive roles for protein domains in trafficking receptors to or away from microvilli have not been established.

1.3.3 Role in Cell Adhesion

The striking characteristics of the surface morphology of leukocytes were intensively investigated concerning their role in cellular adhesion. While definitive

roles of receptor compartmentalization on microvilli remain to be established, commonly two general functions are proposed.

First, prominent villous exposition of adhesion receptors improves the free flowing leukocyte's ability to tether under high shear conditions by increasing the accessibility to its counterreceptors. Indeed, L-selectin transfectants in murine pre-B cells showed impaired tethering capability under flow when expressed on the cell body using a chimera consisting of the ectodomain of L-selectin linked to CD44 (75). This concept was further confirmed by adhesion assays using the same transfectants in lymphoid tissue *in vivo* (86).

Second, the adhesion cascade might require all involved receptors to intervene sequentially (22). Spatial segregation of surface receptors modulating the initial rolling process through microvilli from those mediating arrest and transmigration in the late phase is thought to allow temporal segregation of the adhesion events. Indeed, receptors contributing to the initial events of the cascade such as L-selectin and α_4-integrins are preferentially expressed on microvilli, whereas receptors involved in the late phase such as LFA-1 and MAC-1 are mostly targeted to the cell body.

Reduction of microvilli via cytochalasin B, hypoosmotic swelling or chilling decreased the efficiency of P- and E-selectin-dependent neutrophil tethering (87). Under shear conditions, microvillus stretching as long cylindrical membrane tethers was assigned a major role in lowering the pulling force imposed on the adhesive bonds and extending the bond duration in studies using aspiration micropipette techniques (72). Biophysical simulations also support this conclusion on microvillus deformability in leukocyte rolling (88,89).

These data propose a close relationship between receptor surface topography and function, thus attaching great importance to the microvillus compartment in the context of leukocyte recruitment.

1.3.4 Clinical Relevance

In the past decades, the field of immunobiology advanced dramatically and enforced the revision of traditional concepts of pathophysiology. It occurred that

the immunological system has a much larger medical relevance beyond immunity to microbes and vaccination. Increasing knowledge enabled immunological approaches for cancer therapy, organ transplantation and identified new therapeutic targets for hypersensitivity diseases (e.g. bronchial asthma, food allergies, allergic rhinitis, urticaria) and autoimmune disorders (e.g. systemic lupus erythematodes, Sjögren's syndrome, rheumatoid arthritis, scleroderma). Furthermore, there is mounting evidence of autoimmune and inflammatory components in chronic obstructive pulmonary disease (COPD) and arthrosclerosis (3).

The adhesion cascade during leukocyte migration is central for both physiologic and pathologic situations. Defects in either adhesion step result in a severe inability of neutrophils to migrate to the site of inflammation, in humans referred to as leukocyte adhesion deficiency syndrome (LAD) (90-93). This phenotype can pathogenetically be attributed to distinct molecular malfunctions. A molecular dysfunction of the β_2-integrin subunit CD18 causes the LAD-1. LAD-2 shows a defect in the fucose metabolism resulting in insufficient presentation of sLex motifs. Recently, a new etiopathogenesis of cell adhesion defects in humans named LAD-3 was found. Kindlins are a group of proteins with broad cellular functions including integrin activation. Mutations in the KINDLIN3 gene were found to cause primary activation defects of the β-integrins 1, 2 and 3 (inside-out signaling). All these conditions present a vulnerable immunological state of the organism towards recurrent severe infections with atypical pathogens.

There is strong evidence that L-selectin on activated leukocytes contributes to acute lethal graft-versus-host disease (94) and potentiates tumor metastasis, perhaps by mediating interactions between the endothelium and malignant cells (95,96). The clinical application of heparin in cancer patients is shown to attenuate metastasis (97) and to ameliorate Trousseau syndrome, a tumor-associated recurrent thrombophlebitis (98). These effects could be partly attributed to L-selectin inhibition. Another study concludes that the tumor's potential to disseminate hematogenously is correlated with the amount of microvilli on cancer cells (99). Patients with Wiskott Aldrich Syndrome show a defect in the cell shape modulator Wiskott Aldrich Syndrome protein (WASp)

affecting Arp2/3-mediated actin polymerization (100,101). Interestingly, it is speculated that the clinical symptoms might be attributed to dysmorphic microvillus architecture leading to impairment of L-selectin-dependent leukocyte rolling *in vitro* (102). Furthermore, data of a mouse model showed that treatment and prevention of epilepsy also seem to be correlated to adhesion defects of the blood brain barrier (103). Together, defined spatial segregation of adhesion receptors on the cell surface reflects a broad biological principle decisive for a variety of pathologic processes.

Table 1.3 Integrin-blocking antibodies with clinical significance

Antibody	Antigen	Effect	Indication
Abciximab	Integrin α2bβ3 = glycoprotein IIb/IIIa	Inhibition of platelet aggregation, decreased incidence of ischemic complications	Acute coronary syndrome
Natalizumab	Integrin α4β1	Inhibition of lymphocyte extravasation	Relapsing forms of Multiple Sclerosis, Crohn's disease (only U.S.)
Efalizumab	CD11a = subunit of LFA-1	Inhibition of lymphocyte extravasation	Psoriasis, withdrawal from the U.S. marked 2009

With the identification of proteins involved in cellular adhesion in the 80s and the increasing importance on both physiologic and pathologic immunity, participating key players soon became a potential pharmacological target. Two integrin antagonists as monoclonal antibodies are FDA-approved and constitute an integral part of current therapeutic strategies (Table 1.3). Like with other immunosuppressive drugs, adverse effects can be severe and render the organism more prone to opportunistic infections. Moreover, further functional roles of adhesion receptors beyond adhesion such as cell differentiation and development are being elucidated (104). Balancing reasons for or against clinical administration must therefore be done carefully.

Regarding selectins, several interfering substances are also being investigated but none have been clinically approved. Interfering strategies include monoclonal antibodies, macromolecular carriers of sLex (105) or synthetic dendritic polyglycerol sulfates (106) and the regulation of selectin transcription or post-

transcriptional glycosylation (107). A promising candidate in clinical trials of childhood asthma and psoriasis is the synthetic pan-selectin antagonist bimosiamose (TBC-1269) (108).

In addition to shear condition, receptor-substrate interaction and expression level, the functionality of adhesion receptors is also thought to be regulated by its surface localization (75). Pharmacological interference with the cellular machinery accountable for receptor positioning could therefore have a modulating effect on a variety of cell functions. With regard to the adhesion receptors L-selectin and CD44, homing of lymphocytes to secondary lymphatic tissue or bone marrow could be regulated. Altering the surface positioning of L-selectin on neutrophils might also be a potential means to affect pathologic inflammatory responses in rheumatic diseases. Disruption of the microvillus topology of adhesion receptors could therefore have significant therapeutic benefits.

1.4 Aim of the Study

A hallmark of pathologic inflammation is a dysregulated leukocyte activation leading to extensive extravasation into the surrounding tissue. The adhesion receptor L-selectin is of crucial importance for the adhesion cascade as it initiates the first contact of intravascular freely flowing leukocytes to endothelial counterreceptors in lymphoid tissue. The efficiency of this process depends on the predominant receptor localization of L-selectin on cell surface protrusions, i.e. microvilli and ruffles. Little is known about the mechanisms that contribute to receptor sorting to or away from microvilli. Therefore, this study was designed to address the following aims:

- Construction of domain swapped chimeras between L-selectin (localized on microvilli) and CD44 (on the planar cell body) and establishment of stable human cell transfectants as a tool to further characterize protein domain specific functions.
- Determination of the separate contributions of the extracellular, transmembrane and intracellular domains to ultrastructural receptor positioning (microvilli vs. cell body) by electron microscopy.
- Establishment of a flow chamber system for L-selectin and CD44.
- Impact of L-selectin and CD44 surface topology on the efficiency of cellular adhesion under static and shear conditions.

Due to its crucial function in leukocyte adhesion, L-selectin engagement is considered a major target to alter the cellular response to inflammation. This study is aimed to help clarify basic mechanisms of the ubiquitous principle of microvillus receptor surface segregation on non-polarized cells and its functional impact on cellular adhesion under flow.

2 Results

To evaluate the impact of individual protein domains, chimeric proteins were generated by PCR and subcloned into eukaryotic expression vectors. After transfection into human K562 cells, successful expression was verified via RT-PCR, Western Blot and flow cytometry. Using transmission electron microscopy (TEM) the ultrastructural surface pattern of all wildtype and chimeric proteins was then assessed. As precondition for functional assays, the surface expression levels were tightly adjusted by cell sorting and the flow chamber method for L-selectin and CD44 was established. Ultimately, functional deficits of these adhesion receptors were analyzed under steady and flow conditions.

2.1 Chimeric L-selectin/CD44 Receptors

Both microvillus L-selectin and cell body expressed CD44 are type I transmembrane receptors consisting of an extracellular (EC) N-terminal domain, a single membrane spanning segment (TM) and a intracellular (IC) C-terminal tail. Their similar structural composition in combination with their distinct surface topology constitutes the basis for the domain swapping experiments.

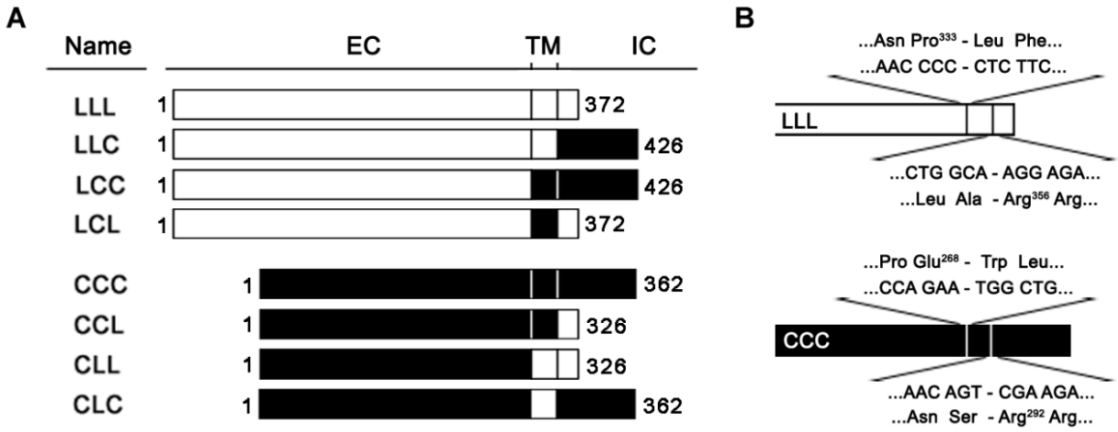

Figure 2.1: L-selectin and CD44 constructs. Domain swapped human L-selectin (open bar) and CD44 (closed bar) receptors. **(A)** Schematic representation of all produced chimeras. Numbers next to the bar indicate the number of amino acids (aa) starting at the NH_2 terminus. Bars are drawn to scale. EC = extracellular, TM = transmembrane, IC = intracellular. **(B)** Amino acid splicing sites at the domain transition zones of L-selectin (open bar) and CD44 (closed bar) used for domain swapping.

Human wildtype L-selectin and human CD44 cDNA were used as templates for the generation of domain swapped chimeric receptors. They are referred to by a three-letter code, each letter representing a protein domain starting at the N- and ending at the C-terminus. While the plasmids containing LLL, CCC, and LCL preexisted, the missing chimeras were produced using a PCR splicing by overlap extension protocol (chapter 4.10.3). It is a genetic engineering technique to construct recombinant DNA with an inserted alteration beyond the limit of practical primer length. Wildtypes and the six mutants were subcloned into the vector pcDNA6, a CMV promoter-driven high copy plasmid, and eventually sequenced to verify their primary nucleotide structure (Figure 2.1). The process of domain swapping is exemplified in Figure 2.2. Other chimeras were generated similarly.

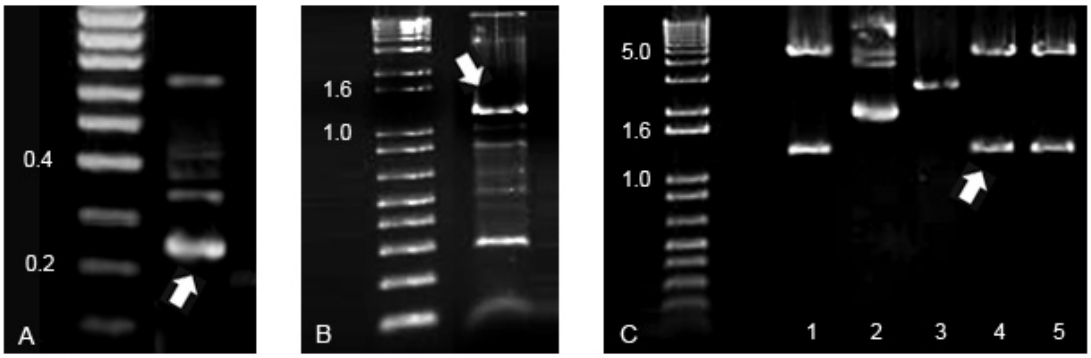

Figure 2.2: Generation of the L-selectin chimera LLC. DNA gel analysis of PCR products. Each left lane represents a mass ladder where numbers indicate the fragment size in kilobases. (A) and (B) The intracellular CD44 domain linked to an overlap extension of the L-selectin transmembrane domain was amplified (size: 235bp, A) and extracted by gel purification. It served then as a reverse primer in a second PCR that fused both fragments resulting in the chimera LLC (size: 1278bp, B). (C) After subcloning the construct into the vector pcDNA6 and transforming it into E.Coli, five clones were picked out of which three turned out correct. Clones 1, 4 and 5 showed the appropriate size of the insert after EcoRV and BamHI digestion. Nucleotide sequencing verified the correct primary sequence, thus excluding point mutations.

2.1.1 Stable Cell Transfection

The human cell line K562 was used as a model system to analyze topological and functional implications of domain swapping. It resembles precursor cells of the human myeloid and lymphoid cell lineage and is L-selectin- and CD44-negative.

For transfection, the electroporation technique was used as described in chapter 4.11. After the antibiotic selection process, the successful integration of the plasmid was verified by RT-PCR (RNA level), Western Blot (protein level) and flow cytometry (surface presentation).

2.1.2 RT-PCR

The successful transfection was shown at RNA level by a reverse transcriptase (RT)-PCR using a forward and reverse primer (Figure 2.3) framing the entire length of the construct. Details on the method can be found in chapter 4.13.

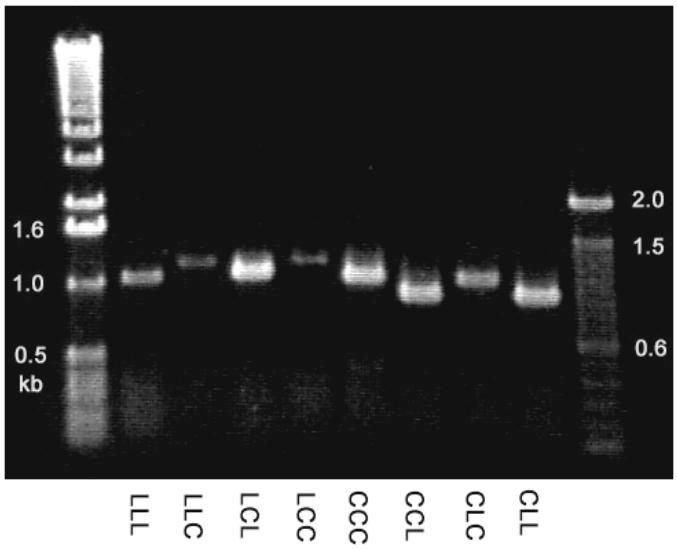

Figure 2.3 mRNA expression of transfected K562 cells. Cell lysates of transfected K562 cells were purified and the mRNA was identified using a RT-PCR with specific forward and backward primers. Different sizes of the chimeras reflect the differing size of the IC domain of CD44 and L-Selectin. A mock transfectant as control showed no band (not shown). More details are provided in chapter 4.13.

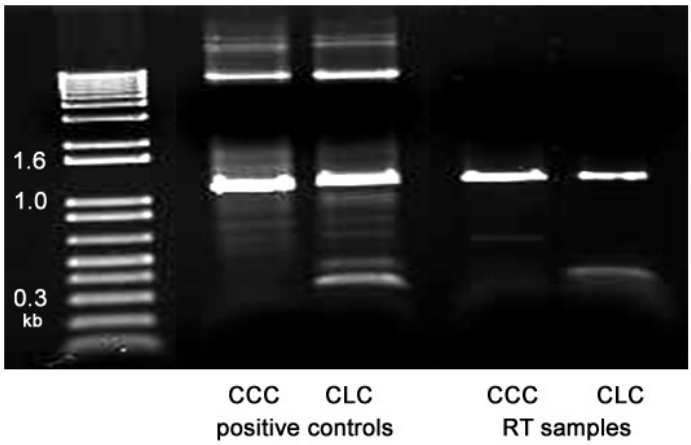

Figure 2.4: Identification of K562 cells transfected with CLC via RT-PCR. Lanes 1 and 2 are positive controls showing the amplification of the cDNA of CCC and CLC. A forward and reverse primer frame the entire chimera resulting in a large band of 1.2kb. The second forward primer only binds at the transmembrane domain of L-selectin and generates, in the case of the chimera CLC, an additional small band of app. 350 bp. The RT samples derive from a reverse transcriptase reaction and amplification of purified cell lysate. Both samples show the main band at 1.2 kb whereas the small band is only seen in the lane CLC indicating their correct identity. The LCL chimeras were identified similarly.

By using an additional third primer (forward) that binds a specific section in the transmembrane domain this method also allows the verification of chimeras with switched transmembrane domains. Because they do not differ in size compared to wildtype (e.g. LLL and LCL) and due to a lack of specific antibodies, RT-PCR but not Western Blot can be used to verify its adequate sequence. Figure 2.4 exemplifies the differentiation between CD44 wildtype and the chimera CLC.

2.1.3 Surface Expression Levels

An important prerequisite of functional adhesion assays is a similar surface receptor expression level of all chimeras to be compared. The measured adhesion rate in a flow chamber is dependent on a variety of factors that ultimately contribute to tethering. This study mainly focuses on receptor positioning as a crucial regulator of adhesive function, thus requiring all other disturbance variables to be minimized. One of them is the amount of plasmid-encoded receptor the transfected cell is presenting on the surface (avidity). While high expression rates account for high tethering in functional assays, low levels cause the opposite and this effect obscures any other subtle ones such as receptor positioning. As a consequence, the receptor surface expression of all cell transfectants to be compared must be roughly similar. Therefore, stable

transfected cell lines were produced allowing the manipulation of the expression levels by cell sorting. With 4 chimeras sharing the same ectodomain and thus adhering on the same ligand, it was intended to match all 4 expression levels. However, due to technical limitations only three (LLL, LLC, LCC) or two (CCC, CLC and CLL, CCL) chimeras were successfully matched.

Cell sorting allows the separation of one cell population into several ones featuring distinct attributes such as cell size, surface receptor profile or expression level. In the context of this study, it was used as a means to match the expression levels of different cell transfectants prior to functional analysis (Figure 2.5).

Flow chamber studies required up to 10×10^6 cells for each experiment, whereas the maximum outcome of a properly sorted population was app. 0.2 – 1.0×10^6 cells. Furthermore, blocking antibodies were used for the fluorescent epitope staining of the cell population to be sorted. It required about 4-6 life cycles of the recultured cells until this blocking effect was negligible in flow chamber experiment. Thus, a regrowing period of about 7 days was necessary after sorting. Despite tight sorting conditions, the recultured cells do not maintain their exact expression levels they were sorted for but rather spread below or above and eventually show an unequal surface expression again. Consequently, for each chimera three different subpopulations with different expression levels were sorted out, marked as low, medium and high (chapter 4.14.3). After culturing them to a confluency high enough to conduct all adhesion assays under flow, matching populations of different chimeras in expression level were identified by flow cytometry just before the experiment. The mean fluorescence intensity (MFI) served as a marker of surface expression identity. Expression histograms of matched populations used for flow chamber studies are shown in Figure 2.5.

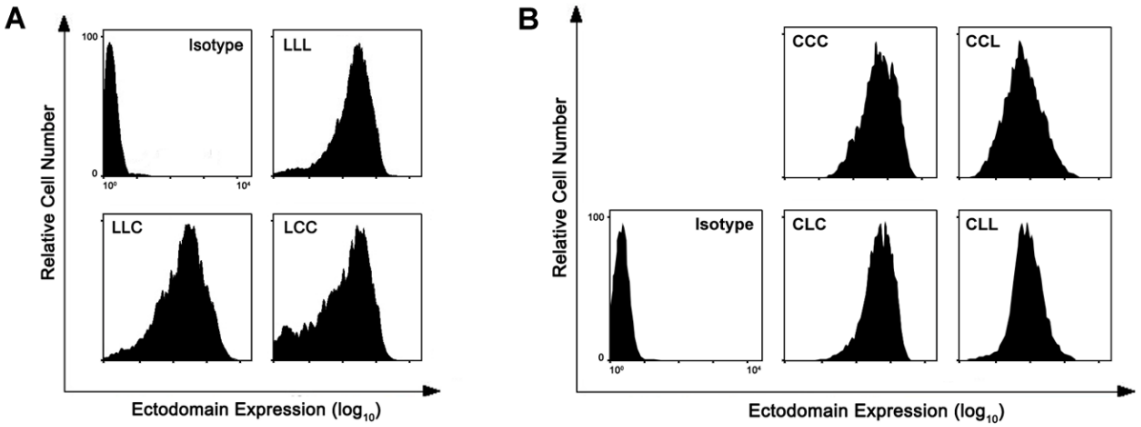

Figure 2.5: Receptor surface expression levels. Flow cytometry histograms showing typical expression levels of L-selectin and CD44 transfectants after cell sorting stained with anti-human fluorescence-labeled mAbs or isotype IgG_1. Only clones with similar surface expression levels were used for functional analysis. LCL could not be properly matched.

2.1.4 SDS-PAGE

Equal amounts of cell lysates of the CD44 and L-selectin chimeras were processed and stained for the respective protein in a Western Blot assay. Western blot analysis is a means to show the correct plasmid expression at protein level. After the specific staining for L-selectin and CD44, the blot was stripped for the 43 kDa loading control β-actin. The equal densities of the bands reflect the similar amounts used for all samples, thus serving as a positive control for a quantitative comparison of protein expression. Notably, all Western blot assays were performed after cell sorting. Hence, all L-selectin and CD44 cell transfectants are equal in their surface expression level (except for LCL). Representative blots are shown in Figure 2.6.

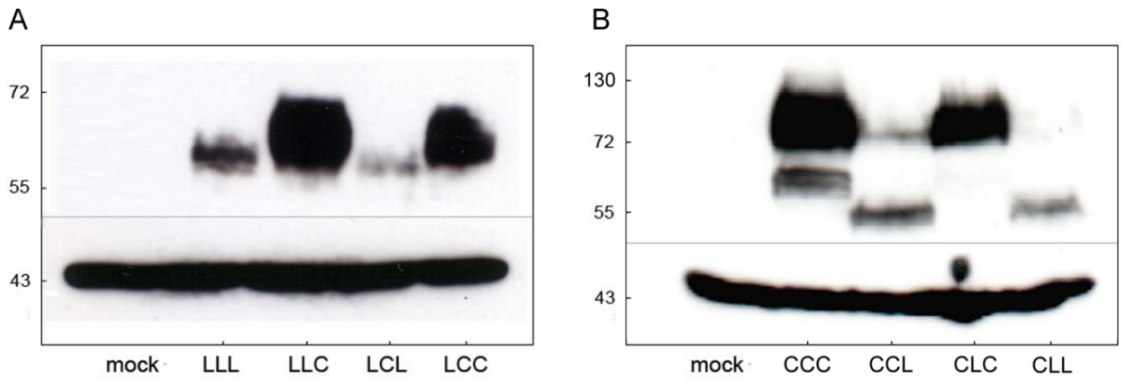

Figure 2.6: Western Blot Analysis. (A) L-selectin and chimeras and **(B)** CD44 and chimeras expressed in human K562 cells. All transfectants show the same receptor surface expression level as shown by flow cytometry except for LCL. Equal amounts of samples were used as verified by the loading control β-actin at 43 kDa (blot strip, bottom). Mock transfected cells served as negative control. Numbers on the left indicate the size in kDa. These blots are representative of two independent experiments.

L-selectin wildtype exhibits a band at ~60 kDa which represents the calculated amino acid backbone of ~37 kDa and cell line specific glycosylation. LLC and LCC exhibit a more intense band. Since the Western blot cannot distinguish molecules exposed on the cell surface or retained in intracellular compartments, the differences may indicate that for LLC and LCC a larger proportion of protein is localized in intracellularly. This could be due to impeded transport to the surface. The increased range up to ~70 kDa might reflect the increasing molecular mass of ~4 kDa upon exchanging the small L-selectin IC domain with the 36 aa larger one of CD44 (calculations based on an average molecular weight of a amino acid of 110 Dalton).

CD44 wildtype has a predicted size of ~ 85 kDa with a potential increase up to 200 kDa through extensive glycosylation. Here, the apparent molecular mass is ~ 80-90 kDa of CCC and CLC and ~ 55 kDa for CCL and CLL. These apparent changes in mass are important insofar as the degree of glycosylation can affect ligand binding characteristics with altered protein function.

Since the Western blot cannot distinguish between molecules exposed on the cell surface or retained in intracellular compartments, the differences found may indicate that for LLC and LCC a larger proportion of protein is localized intracellularly. This could be due to impeded transport to the surface.

2.2 Ultrastructural Receptor Topography

Optical microscopy is limited by the wavelength of the light which allows a maximum resolution of about 0.2 µm. However, cytoplasmic protrusions can be as thin as 0.05 µm. Therefore, the topographic distribution of L-selectin, CD44 and their respective domain swapped chimeras on the cell's surface was assessed by transmission electron microscopy (TEM). A preembedding immunogold labeling technique ensured ultrastructural preservation of the specimen (109). Mock transfectants and cell transfectants labeled only with the secondary gold-bearing antibody showed no staining. No morphologic difference of the microvillus architecture of any cell transfectants was observed. Figure 2.7 shows the morphology of unstained K562 cells and emphasizes the fact that the amount of microvilli seen is heterogeneous and also dependent on the section plane. Therefore, only micrographs allowing clear differentiation between microvilli and cell body were used and special emphasis was put on double blind image acquisition and analysis (chapter 4.15).

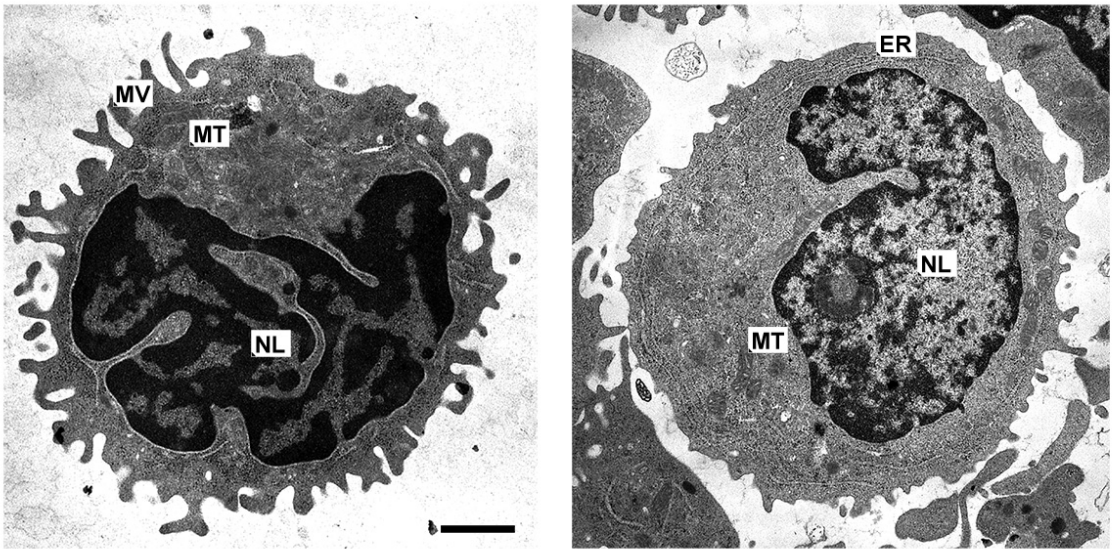

Figure 2.7: Electron micrographs of wildtype K562 cells. Typical micrographs of human myeloid K562 cells acquired by transmission electron microscopy at a magnification of 30.000×. The nucleus is lobulated resembling the myeloid blood cell linage. The diameter of native K562 cells is roughly 13 µm. MV = microvilli, MT = mitochondria, NL = nucleus with euchromatic (light) and heterochromatic (dark) regions, ER = endoplasmic reticulum. Scale bar depicts 2µm.

2.2.1 Impact of the Intracellular Domain

L-selectin (CD62L) and CD44 show a clearly distinct cell surface topology being localized either on microvilli and the cell body, respectively. Since published data mainly emphasize cytoplasmic interactions in determining surface positioning (chapter 1.3.2), the question whether the IC domains of L-selectin and CD44 affect surface distribution was first addressed.

Consistent with previous findings (75), 88% of L-selectin (LLL) was associated with microvilli, whereas CD44 (CCC) concentrated on the planar cell body in K562 cells. Surprisingly, the substitution of either cytoplasmic tail did not have significant effects on surface topology. LLC was still predominantly positioned on microvilli and CCL was found on the cell body at a degree similar to the respective wildtypes (Figure 2.8, Figure 2.9, Figure 2.10 and Table 2.1).

2.2.2 Impact of the Transmembrane Domain

The unchanged distributions of LLC and CCL compared with LLL and CCC suggest that the motif for the surface localization of L-selectin and CD44 may be encoded in their outer segments. Previous work had established that swapping the EC domains alone had no effect (75). We confirmed this finding since the chimera LCC remained on the planar cell body and CLL was expressed on microvilli in a ratio similar to CCC and LLL, respectively. These findings, in conjunction with the result that swapping of the IC domain did not have significant effects on cell surface topology, suggest that the TM domain may be a major determinant of L-selectin and CD44 surface presentation.

To examine this hypothesis, chimeras with a replaced TM but unmodified IC and EC segment were generated (Figure 2.1). Indeed, substitution of L-selectin's TM domain (LCL) provoked a significant loss of the microvillus localization, with 80% of all labeled proteins found on the planar cell body and excluding microvilli (Figure 2.8), similar to CD44's typical surface distribution. Likewise, CLC was hardly found on the planar cell body but showed a major shift to the microvillus compartment (Figure 2.9). Detailed data is provided in Table 2.1.

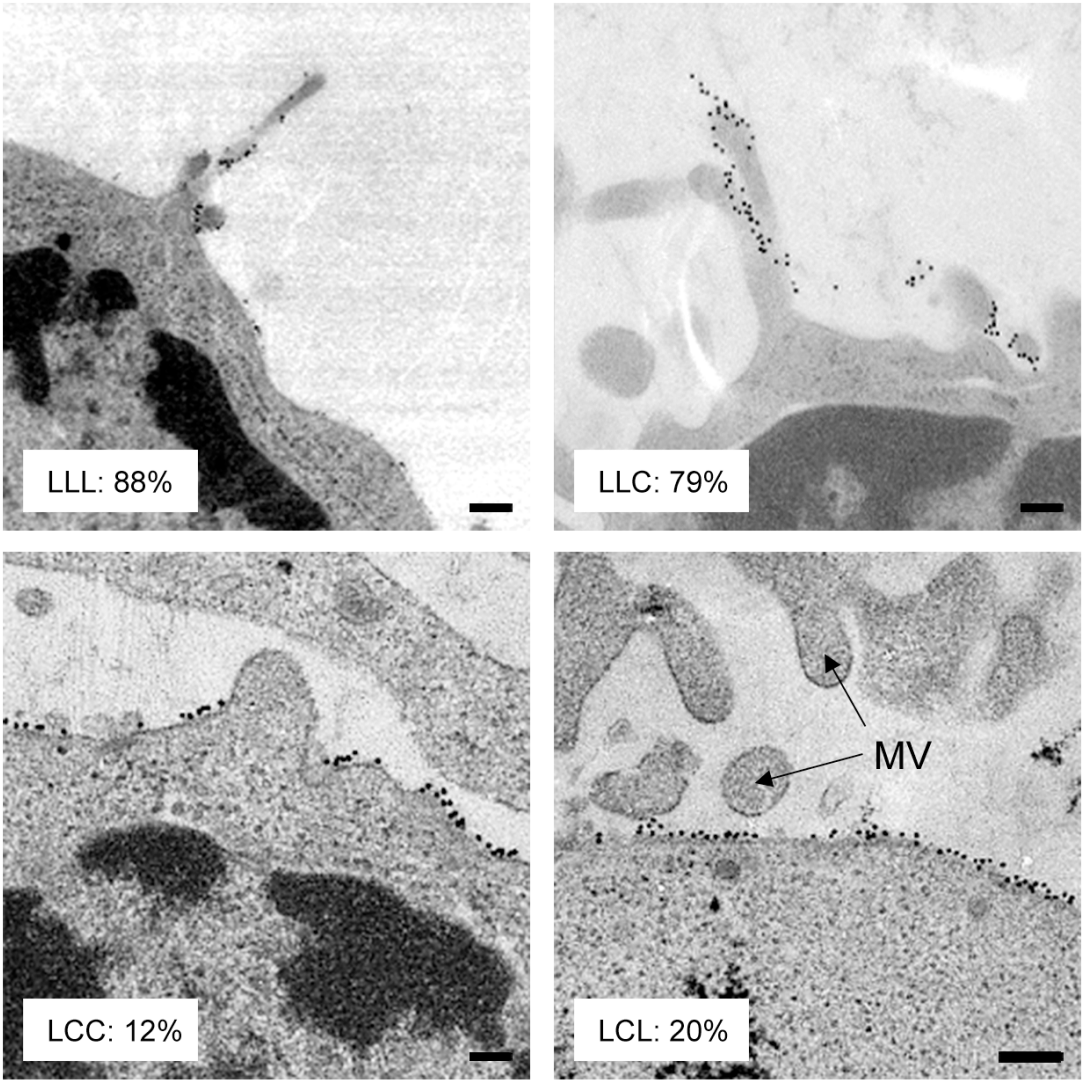

Figure 2.8: Receptor cell surface topography of L-selectin constructs. Transfected K562 cells expressing human wildtype L-selectin (LLL) or chimeric receptors were analyzed for their surface localization using immunogold-labeling (black dots) and transmission electron microscopy. Representative surface patterns with their mean percentage distribution on microvilli of L-selectin transfectants are shown. LCL expression about half as high as LLL, LLC, LCC. Detailed data is provided in Table 2.1. Scale bars depict 0.1 µm.

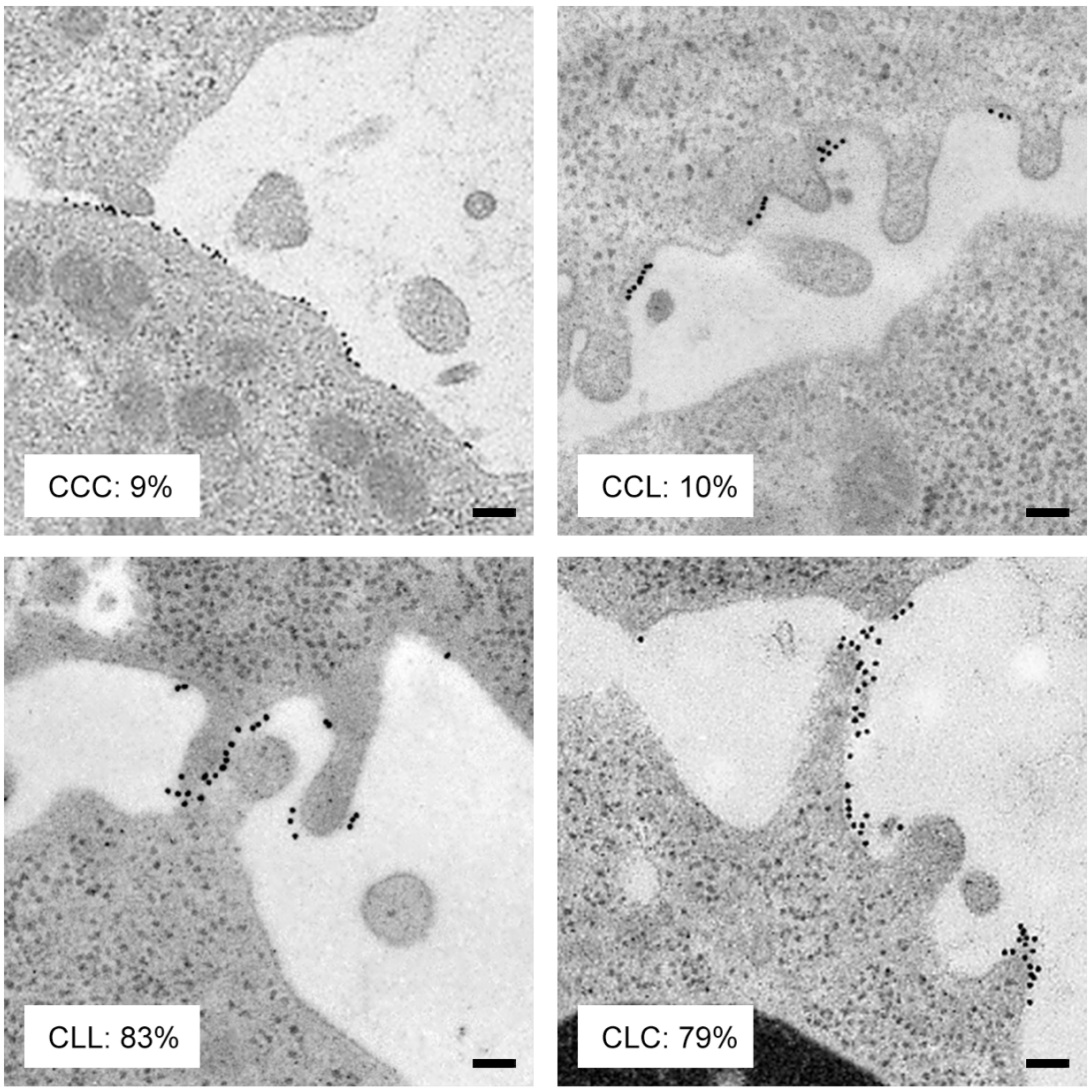

Figure 2.9: Receptor cell surface topography of CD44 constructs. Transfected K562 cells expressing human wildtype CD44 (CCC) or chimeric receptors were analyzed for their surface localization using immunogold-labeling (black dots) and transmission electron microscopy. Representative surface patterns with their mean percentage distribution on microvilli of CD44 transfectants are shown. Detailed data is provided in Table 2.1. Scale bars depict 0.1 µm

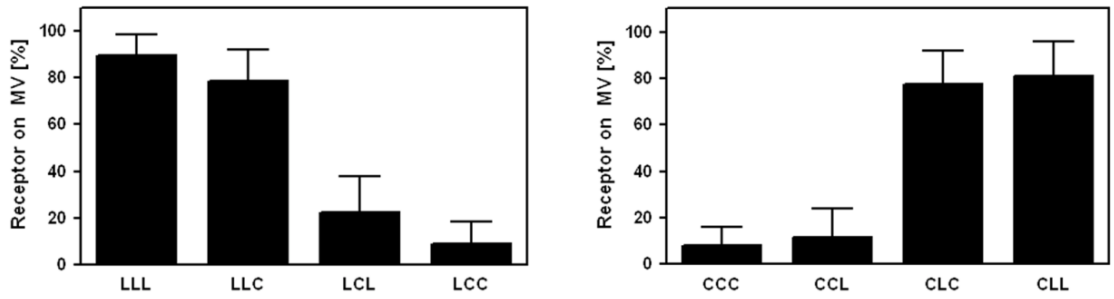

Figure 2.10: Transmission electron microscopy analysis of the surface receptor localization of L-selectin / CD44 chimeras in transfected K562 cells. Image acquisition and analysis of the 10 nm colloidal gold distribution was performed by two independent blinded observers at a magnification of 30.000 – 60.000×. Mock transfected cells did not show any staining. Data is presented as mean ± SD of two experiments performed in duplicates.

Table 2.1 Surface distribution of L-selectin and CD44 wildtypes and chimeras expressed in human K562 cells as analyzed by transmission electron microscopy.

Receptor	Distribution (%)			Total Number Analyzed	
	Microvilli	***Cell Body***	***p*[a]**	***Gold Particles***	***Cells***
LLL	88 ± 10	12 ± 10	—	1310	20
LCL	20 ± 15	80 ± 15	< 0.01	1104	24
LLC	79 ± 13	21 ± 13	NS	1445	18
LCC	12 ± 9	88 ± 9	< 0.01	1318	26
CCC	9 ± 8	91 ± 8	—	785	21
CLC	79 ± 15	21 ± 15	< 0.01	1289	31
CCL	10 ± 12	90 ± 12	NS	1123	24
CLL	83 ± 15	17 ± 15	< 0.01	1069	25

a Significance of difference to wildtype (one-way ANOVA, Dunnett's post hoc test)

2.3 Adhesion under Static Conditions

Electron microscopy studies revealed that the transmembrane domains of L-selectin and CD44 determine receptor surface distribution in human K562 cells. This allows the functional comparison of two receptors that share the same extracellular ligand binding domain but differ in their preferred membrane position (microvilli vs. cell body). The determination of the impact of receptor position on

cell adhesion under flow requires that the modification of the receptor domains does not have any influence on ligand binding whatsoever (e.g. through conformational changes). Therefore, static binding assays were conducted to show that ligand binding itself is not diminished by swapping the transmembrane and intracellular protein domain.

2.3.1 Flow Cytometry Titration

DREG-56 antibodies bind a precise region of the L-selectin lectin domain responsible for ligand binding (38) and can therefore be used as a ligand blocking antibody. Reduced mAb affinity as a result of domain swapping could indicate possible alterations in secondary or tertiary structure of L-Selectin. To increase sensibility of the assay, a concentration gradient of mAbs was used and the affinity was determined using flow cytometry. It is assumed that antibodies have equal access to the entire cell surface irrespective of the ultrastructural surface localization.

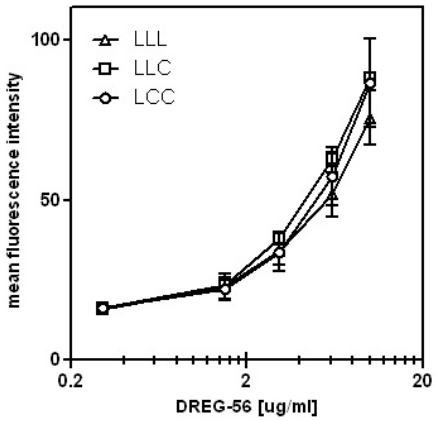

Figure 2.11: Differential binding of L-selectin and chimeras. Flow cytometry titration of L-selectin transfectants using the anti-human L-Selectin MAb DREG-56 in the range of 0.3 to 10 µg/ml. Mean fluorescence intensity (MFI) shows the percentage of cells stained with DREG-56 and is corrected for background staining of mock transfectants. Data shows mean ± SD of two independent experiments in duplicates.

In the range of 0.3 to 10.0 µg/ml, the chimeras LLC and LCC showed similar binding affinity as wildtype L-selectin (Figure 2.11). This data shows that the endogenous ligand affinity of LLL, LLC and LCC is equal in binding DREG-56.

2.3.2 Adhesion on Immobilized Ligands

To address the functional implications of surface localization, transfectants with tightly matched surface expression levels were established which was successful for all constructs except LCL (Figure 2.5). Static binding of wildtype L-selectin and chimeras was assessed using immobilized PSGL-1, a known ligand for L-selectin (110). Cells were allowed to settle on coated hydrophobic glass slides, washed and the number of bound cells was counted. In agreement with Figure 2.11, no significant difference in binding activity between the N-terminal ligand binding lectin domains of L-selectin wildtype and chimeras could be detected (Figure 2.12A). Similarly, the static adhesion activity of the CD44 transfectants was investigated using its physiologic ligand hyaluronan (66), showing no evidence for differential adhesion (Figure 2.12B). This is particularly important as Western Blot analysis hints at possible alterations in glycosylation (chapter 2.1.4) that can affect ligand binding.

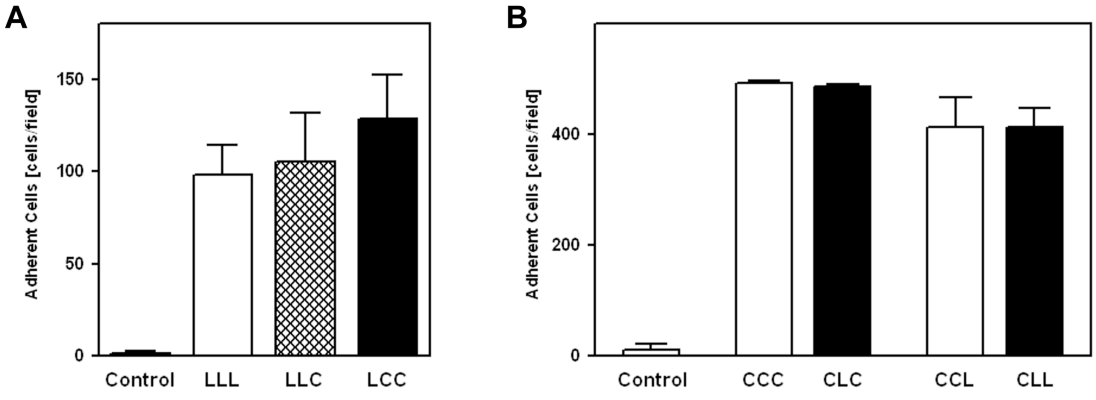

Figure 2.12: Static adhesion of K562 transfectants. (A) Static binding of L-selectin transfectants to immobilized PSGL-1 on hydrophobic glass slides. The specificity of binding was confirmed by cells preincubated with blocking DREG-200 mAb (Control). Mean ± SD of five independent experiments. (B) CD44 cell transfectants bound to hyaluronan under static conditions. Blocking anti-CD44 mAb served as control. CCC and CLC express closely matched surface expression levels, as do CCL and CLL. Data presented as mean ± SD of three independent experiments.

2.4 Adhesion under Flow

2.4.1 L-Selectin Adhesion on PSGL-1

L-selectin supports fast leukocyte rolling on PSGL-1 (111,112), whereas CD44 mediates very slow rolling on hyaluronan (66). Therefore, clones with similar

surface expression levels were used to assess rolling flux and velocity for all L-selectin assays and cell accumulation for CD44 assays, respectively. To mimic leukocyte-endothelium interactions, a parallel plate flow chamber was employed allowing the characterization of the adhesion behavior under defined wall shear stress conditions.

Calibration of the Flow Chamber

A threshold L-selectin ligand concentration is required to keep up an ongoing receptor-ligand interaction resulting in transient cell rolling (41). Preliminary experiments were conducted to determine the optimal coating concentration for L-selectin-dependent rolling (Figure 2.13). With the recombinant ligand PSGL-1-IgG used in this study, a coating concentration of 10 µg/ml was not sufficient to support rolling, whereas 75 µg/ml or higher supported steady rolling. However, coating concentrations below 150 µg/ml required an equilibration time in order to reach a steady rolling state. Therefore, all L-selectin flow chamber assays were carried out with a PSGL-1 coating concentration of 150 µg/ml.

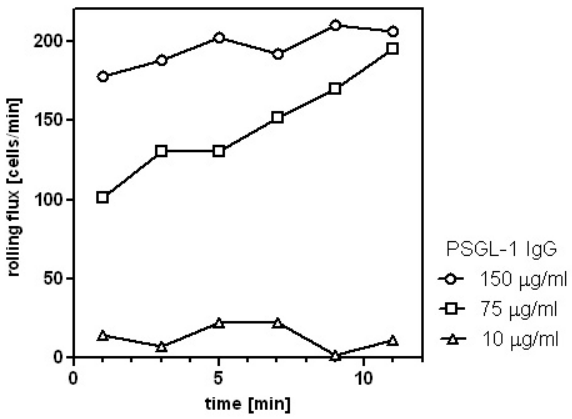

Figure 2.13: L-selectin rolling at varying PSGL-1 coating concentrations. L-selectin wildtype transfectants rolling on PSGL-1 using increasing coating concentrations of the ligand at a shear stress of 1 dyn/cm^2. Time point 0 indicates the start of the experiment. Data is not comparable with **Figure 2.14** because the receptor surface expression of cell transfectants used is not equal. Data representative of multiple preliminary experiments.

Adhesion Assay

L-selectin showed efficient tethering and subsequent rolling on PSGL-1 at shear stresses between 0.7 and 2.3 dynes/cm^2. Below 0.7 dynes/cm^2 the rolling flux

was severely reduced reflecting the shear threshold property of L-selectin bonds (41) (not shown). Both mock transfectants and the blocking anti-L-selectin mAb DREG-200 were employed as specificity controls and completely abolished all interaction.

Consistent with published data (75), the cell body-based chimera LCC showed a severely reduced rolling flux compared to microvillus-expressed LLL. LLC showed an intermediate phenotype between LLL and LCC at all tested shear rates (Figure 2.14). LCL was not included because the surface expression level could not be matched. Detailed data is provided in Table 2.2.

After having shown that ligand binding is not negatively affected through protein domain swapping, significant functional deficits are analyzed under shear conditions. Apparently, the application of physiological shear stress emphasized major differences in ligand binding. Compared to wildtype, intracellular and transmembrane swapping accounts for about 50% and 80% loss in adhesion, respectively. While LLL was best adapted to initiate adhesion under shear conditions, changes in the IC and TM domain lead to reduced ligand adhesion.

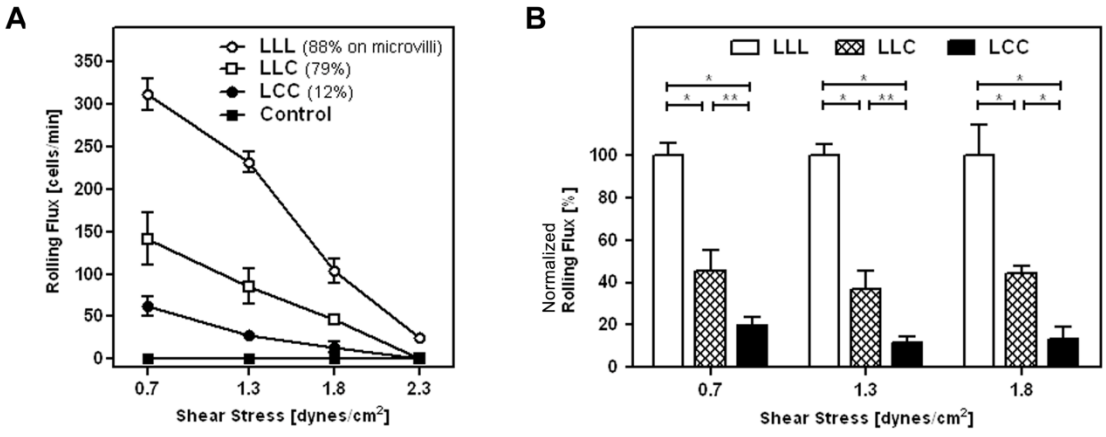

Figure 2.14: Rolling of L-selectin transfectants on PSGL-1. Rolling on PSGL-1 of K562 cells transfected with L-selectin wildtype (LLL) and chimeras LLC and LCC was examined under different shear conditions. The compared cell lines shared a similar surface expression level (**Figure 2.5**). (A) Steady-state rolling flux. Cells incubated with the blocking anti-human DREG-200 mAb served as negative control. Data are presented as mean ± SD of five independent experiments. (B) Same data, but normalized to rolling flux of LLL (=100%). * $p < 0.002$, ** $p < 0.015$ (paired t test, n = 5 in each group)

Table 2.2: Rolling of K562 transfectants on recombinant PSGL-1. Rolling of L-selectin wildtype and chimeras rolling on PSGL-1 was examined at low, medium and high shear stress. Rolling flux data represent 5 independent experiments. n indicates the number of cells analyzed for rolling velocity.

Shear stress	Receptor	Rolling Flux	Rolling Velocity		
[dynes/cm^2]		Mean ± SD [cells/min][a]	Mean ± SD [µm/s][b]	Median [µm/s]	n [cells]
0.7	LLL	312 ± 18	103 ± 58	93	88
	LLC	142 ± 30[c]	107 ± 58	109	87
	LCC	62 ± 12[c]	120 ± 56	112	33
1.3	LLL	232 ± 12	116 ± 67	113	75
	LLC	85 ± 21[d]	117 ± 59	111	71
	LCC	27 ± 6[c]	133 ± 67	126	29
1.8	LLL	104 ± 15	119 ± 70	104	72
	LLC	46 ± 4[c]	131 ± 80	115	65
	LCC	14 ± 6[c]	138 ± 46	131	28

[a] Cells during steady-state rolling crossing a virtual perpendicular line of 1 mm length within 1 min.

[b] The velocity of steadily rolling cells was analyzed using a MATLAB snake model tracking algorithm.

[c] $p < 0.002$ and [d] $p < 0.015$ compared with LLL (paired t test); n = 5 at each condition.

Rolling Velocity

Leukocyte adhesion receptors initiate cell rolling with a characteristic velocity depending on the ligand they are interacting with. The velocity of cells rolling on PSGL-1 was calculated by a snake cell tracking algorithm using MATLAB. Due to the high speed camera deployed for recording, a high resolution velocity profile of each individual rolling cell could be generated showing the microkinetics of the receptor substrate interaction (Figure 2.15).

Because of different receptor surface expression levels and the changing shear stress gradient along the width of the channel, the characteristic rolling velocity of a cell population needs to be determined by analyzing a representative cohort of rolling cells. A frequency distribution histogram allows the visualization of statistical key data such as median, standard deviation and minimal and maximal value. Therefore, a histogram overlay is used to compare the velocity profile of two or more cell populations.

Velocity calculations were performed only for L-selectin transfectants as CD44-hyaluron interactions do not support rolling. For each chimera, 28 to 88 cells were tracked at 0.7 or 1.8 dynes/cm^2 and visualized in a cumulative frequency histogram (Figure 2.16). Detailed statistical data is noted in Table 2.2.

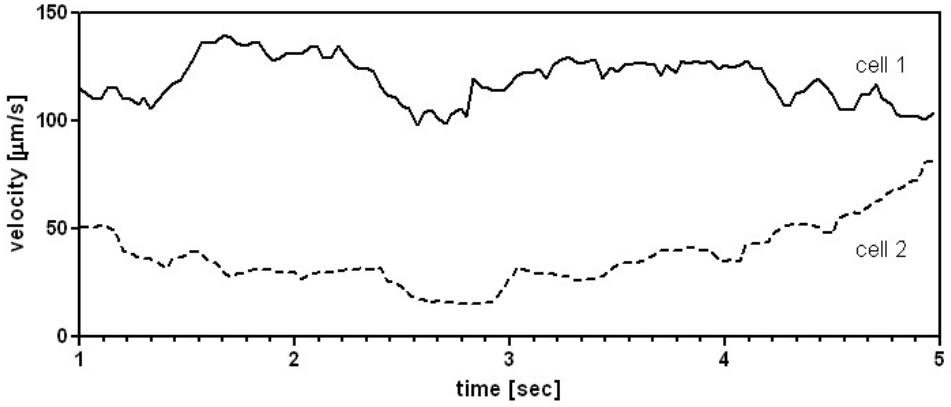

Figure 2.15: High resolution velocity profile of rolling L-selectin transfectants. K562 cells transfected with L-selectin wildtype rolling on PSGL-1 at 1 dyn/cm^2. Video capturing was performed with 30 frames per second enabling a velocity analysis at a resolution of 30 datapoints per second. The average velocity of cell 1 is 121 µm/s and of cell 2 46 µm/s.

The microkinetic analysis of cells rolling through L-Selectin PSGL-1 interactions showed that individual cells vary in their velocities over time. This phenomenon of non-homogenous velocity profiles in this experimental setup is significant insofar as valid mean velocities can only be measured with a timeframe long enough to compensate the oscillation. Here, mean velocities were calculated only using cells that show steady rolling of 4 seconds or longer.

Wildtype L-Selectin (LLL) shows a velocity range from ~20 µm/s up to ~250 µm/s with a mean of ~100 µm/s. This range is likely to represent different surface expression levels of L-Selectin on different cells of the population. An increase of the applied shear stress from 0.7 dynes/cm^2 to 1.8 dynes/cm^2 does not lead to a significant shift to higher velocities. The chimeras LLC and LCC present similar data with only slightly higher velocities. However, these changes are non-significant in the cohorts used.

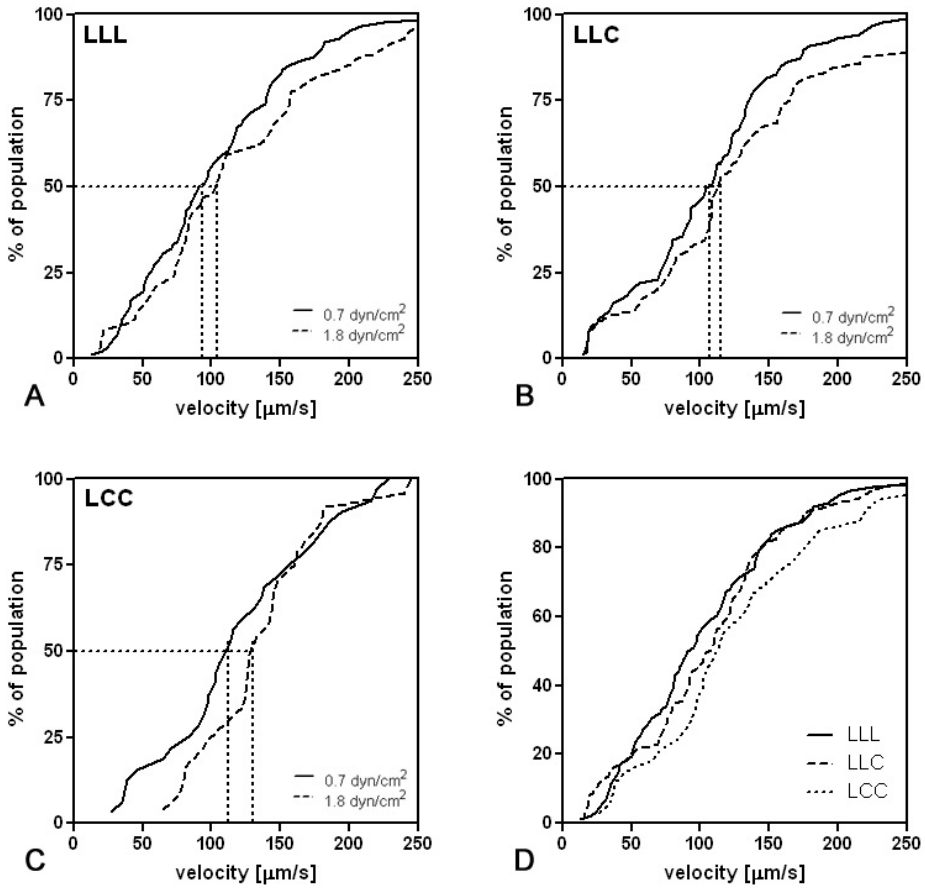

Figure 2.16: Velocity profile of L-selectin transfectants. Cumulative frequency histograms showing the velocity profile of L-selectin transfectants at low and high shear conditions (A, B, C). Small dotted line at 50% indicates the median. (D) Comparison of wildtype L-selectin and chimeras LCC and LLC at a low shear stress of 0.7 dynes/cm^2. The number of cells analyzed, the mean and the median are indicated in Table 2.2.

2.4.2 CD44 Adhesion on Hyaluronan

Next, the impact of microvillus positioning of CD44 on cell adhesion was investigated. Expression-matched pairs of CCC and CLC as well as of CLL and CCL were compared in a flow chamber assay.

Calibration

CD44 interaction to hyaluronan as a main in vivo ligand (62) supports adhesion highly dependent on the applied shear stress. Preliminary experiments were conducted in order to determine an appropriate shear stress level that clearly allows sufficient binding without quickly reaching a saturated plateau. Figure 2.17

shows a shear gradient of K562 cells transfected with wildtype CD44 over time indicating that subtle differences in shear cause major changes in adhesion.

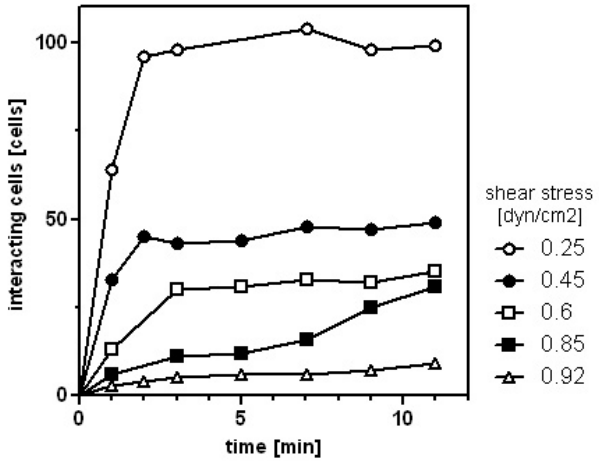

Figure 2.17: CD44 adhesion to hyaluronan at different shear conditions. K562 cells transfected with CD44 wildtype were subjected to shear ranging from 0.25 to 0.92 dynes/cm^2 in a parallel flow chamber assay. 0.5 x 10^6 cells/ml were used and the amount of sticky cells within a field of 1 mm^2 counted over time. Results are not comparable with Figure 2.18 due to different cell concentrations and to different receptor expression levels. Blocking CD44 mAb were used as a negative control. Data representative of two similar experiments.

Adhesion Assay

With emphasis on the TM domain, expression-matched pairs of CCC and CLC as well as CLL and CCL, respectively, were compared in a flow chamber assay (Figure 2.18). In both cases, microvillus-expressed CD44 receptors (CLC, CLL) supported approximately 3-fold more adhesion than the cell body-based counterparts (CCC, CCL). Note that both pairs feature the same cytoplasmic tail and thus have the same cytoplasmic anchorage.

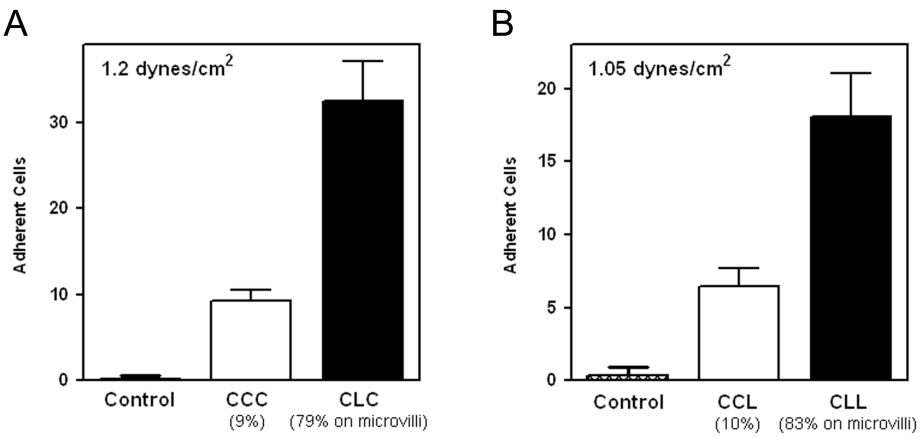

Figure 2.18: Accumulation of CD44 transfectants on hyaluronan under flow. Rolling and adherent K562 cells transfected with (A) CCC or CLC and (B) CCL or CLL were counted 7 minutes after the initiation of flow within a field of 1 mm^2 in a flow chamber setup. Each pair of cell lines shared a similar receptor surface expression level (Figure 2.5). Accumulation of mock transfectants (Control) was negligible. All bars show mean ± SD of three independent experiments.

3 Discussion

In this study the topography of L-selectin and CD44 wildtype and chimeras with swapped EC, TM and IC domains was compared in order to determine the impact of different protein domains on ultrastructural receptor localization on the cell surface. Chimeras were generated via a PCR technique and stably transfected human myeloid cells were immunogold-labeled and analyzed via electron microscopy. The receptor functionality was then examined to analyze whether or not surface localization of these adhesion molecules is relevant for biological function. This was done by adhesion assays under static and physiologic flow conditions using a flow chamber.

3.1 Microvillus Receptor Positioning

Statistical analysis of the receptor distribution showed that 88% of wildtype L-selectin (LLL) was associated with microvilli, whereas wildtype CD44 (CCC) concentrated on the planar cell body. This is consistent with previous data by Bruehl et al. and von Andrian et al. using transmission and scanning electron micrographs, respectively (39,75), and by Hocdé et al. using total internal reflection microscopy (82). Therefore, K562 cells bear the complete molecular mechanisms required to properly present L-selectin and CD44 on the surface as observed in other cells.

3.1.1 Intracellular Interactions

Using TEM, no significant impact of the IC tail could be detected for L-selectin or CD44 suggesting that cell surface positioning at least of these two receptors is not determined by cytoplasmic interactions. LLC was still predominantly positioned on microvilli and CCL was found on the cell body at a degree similar to the respective wildtype (Figure 2.8 and Figure 2.9). Previous studies had shown that mutations of ERM binding residues within the proximal IC domain of L-selectin abolish expression on microvilli (84) but deleting its ERM-distal cytoplasmic tail does not (85). This leads to the assumption that ERM association of L-selectin is necessary for microvillus positioning. The fact that the IC domain

of CD44 also contains an ERM binding site (113,114) might be a possible explanation for the unchanged topography of LLC compared to LLL. Likewise, mutations of the intracellular ERM binding residues of CD44 do not interfere with surface localization (64). Therefore, ERM linkage of compartmentalized cell surface receptors seems not to be sufficient for defining their sorting to membrane protrusions or to the cell body.

3.1.2 Intramembranous Interactions

The unchanged distributions of LLC and CCL compared with those of LLL and CCC suggest that the motif for the surface localization of L-selectin and CD44 may be encoded in their transmembrane or in their extracellular segments. Previous work had established that swapping the EC domains alone had no effect (75). We confirmed this finding, since the chimera LCC remained on the planar cell body and CLL was expressed on microvilli in a ratio similar to LLL. These findings in conjunction with the result that swapping of the IC domain did not have significant effects on cell surface topology suggested that the TM domain may be a major determinant of L-selectin and CD44 surface presentation.

Indeed, substitution of L-Selectin's TM domain by that of CD44 (LCL) provoked a significant loss of the microvillus localization, with 80% of all labeled proteins found on the planar cell body and excluding microvilli, similar to CD44's typical surface distribution. Likewise, hardly any CLC was found on the planar cell body but instead showed a major shift to the microvillus compartment (Figure 2.8, Figure 2.9 and Table 2.1).

In polarized cells, selective targeting and intracellular stabilization at the basolateral and apical cell surface are two putative mechanisms responsible for cell polarization inducing the formation of biochemically and functionally distinct plasma membrane domains (115). Asymmetric distribution of protein and lipids requires tight junctions in the *zona adherens* that serve for intercellular adhesion and constitute a physical border of the cell membrane. This is especially important in the microarchitecture of the kidney because transport processes that ensure homeostasis rely on the principle of cell polarity. Abnormal apical membrane polarity is the pathogenetic cause for autosomal dominant polycystic

kidney disease (ADPKD). Among the factors mediating cell polarization are three evolutionary conserved complexes called Crumps, Par and Scribble (116-118). A complex network of pathways is involved in directing proteins to the apical or basolateral domain, including the polarization complexes as well as Small GTPase rab proteins as master regulators (119).

Epithelial cells bear microvilli on their apical site whereas the basolateral compartment remains rather flat, resembling the protrusive or the flat subdomains on leukocytes, respectively. Receptors of blood-borne non-polarized cells may be compartmentalized by cognate sorting mechanisms (120). Given our findings, it seems that leukocyte receptor compartmentalization involves two functionally separate processes: selective targeting via the TM domain and perhaps unspecific stabilization through intracellular ERM linkage of both CD44 and L-selectin to the cytoskeleton.

CD44's and L-Selectin's TM domains are both 95-100% conserved among mammalian species (Figure 3.1). This observation strongly indicates that these TM helices indeed take center stage in physiologic receptor function e.g. by defining surface localization. E-Selectin, another member of the selectin family, is displayed ubiquitously on the surface of pre-B cell transfectants including flat and protrusive sections (75). Despite the close relationship to L-Selectin in the EC domain, its TM domain is barely conserved in mammals. Thus, it is plausible to propose that non-compartmentalization of leukocyte surface receptors constitutes a "default pathway", while TM signals lead to an active segregation to the cell body or microvilli.

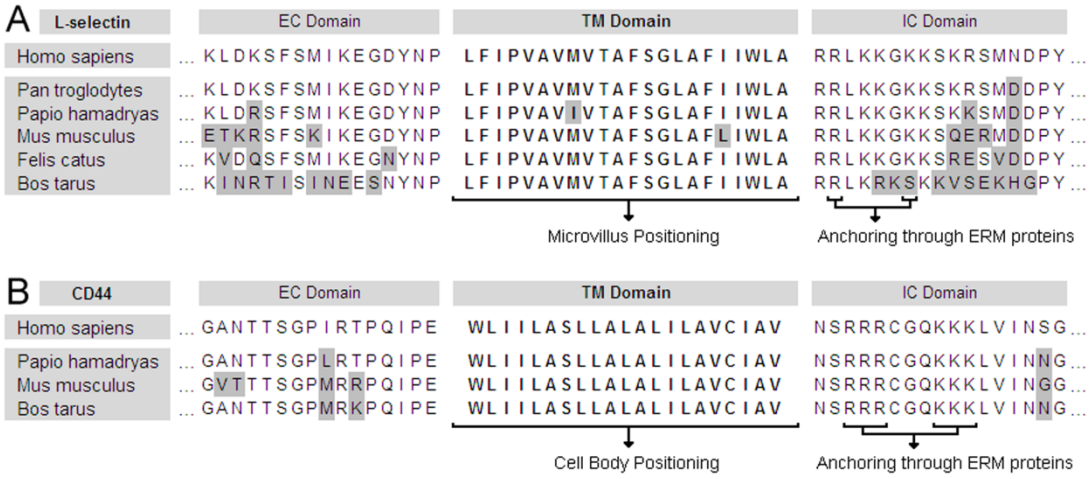

Figure 3.1: Phylogenetic comparison of L-selectin's and CD44's membrane-spanning regions. Primary amino acid sequences of different species are depicted with their predicted IC and TM domains along with the adjacent beginning of the EC segment. Single mutations differing from *Homo sapiens* are highlighted gray. The vertical order roughly reflects the taxonomic distance to *Homo sapiens* (from top to bottom). ERM binding residues are indicated according to Ivetic et al. (2004) and Legg and Isacke (1998). For multiple sequence alignment, the program ClustalW2 was used with default settings.

Role of Lipid Raft Integrity

Research about the organization of the plasma membrane has focused on cholesterol-enriched microdomains (lipid rafts) as a main constituent of distinct subdomains. The tyrosine kinase $p56^{Lck}$ was shown to play a central role in trafficking the CD4 receptor to microvilli in the lymphoid cell line CEM (121). Notably, lymphocyte L-selectin requires functional $p56^{lck}$ for the activation of the Ras-pathway (122). Moreover, a PSGL-1 mutant lacking the IC tail and thus missing a putative ERM binding domain still concentrates on microvilli of primary leukocytes (77). As this mutant was still able to associate with lipid rafts and promote normal rolling on P-selectin, the authors hypothesized that cytoskeletal anchorage of PSGL-1 was achieved through raft molecules that, in turn, link to actin. Similarly, the deletion of the C-terminal cytoplasmatic tail of prominin, a pentaspan TM glycoprotein associated with lipid rafts, does not perturb its accumulation on microvilli (123). Collectively, these findings support the concept of lipid raft integrity as a precondition for microvillus receptor presentation. However, other studies seem to contradict: cell body CD44 in murine fibroblasts (124) but not microvillus L-selectin in human primary cells (125) was shown to be enriched in rafts using the detergent Triton X-100. This incongruence could be

due to cell type-specific discrepancies, the existence of multiple mechanisms for protein sorting or multiple types of rafts populating different surface subdomains.

Fundamentally new insights derived from a study describing the coexistence of multiple cholesterol-based raft-like subsets that occupy distinct membrane subdomains in the apical membrane of MDCK cells (126). Since this study enforces the concept of lateral membrane interactions as the unique determinant for surface localization, other than Triton X-100 soluble cholesterol rafts (e.g. Lubrol WX) should also be considered to play a role in leukocyte receptor compartmentalization. If so, this would signify an important link between the cholesterol metabolism and the homeostasis of the immune system.

3.1.3 Diversity of Mechanisms

The complexity of microvillus receptor expression is further illustrated by the failure to display human wildtype PSGL-1 on microvilli in transfected K562 cells (127) but not in primary cells (77,78). This points to possible accessory molecules necessary for PSGL-1, but not L-selectin positioning. Similarly, the CD44 receptor localizes to the planar cell body of L1-2 pre-B cells (75), but not of a melanoma cell line where it colocalizes with Ezrin in microvilli (64). Furthermore, domain swapping experiments of α_4- and β_2-integrins (on microvilli and on the cell body, respectively) suggest that EC interactions may be responsible for microvillus positioning (80). The fact also that microvillus membrane protrusions are highly dynamic with an average life time of 12 min according to in vivo scanning ion conductance microscopy studies should be taken into account (73). Taken together, despite a very similar phenotype, the underlying mechanisms for the association of different surface receptors with microvilli seem to be diverse.

3.1.4 Functional consequences

As a precondition for functional flow assays, the ability of the constructs to bind ligand was compared in a static environment. Neither receptor surface topology nor domain swapping influenced the adhesive function of L-selectin or CD44 under static conditions (Figure 2.12). To avoid an avidity bias in functional

assays, the receptor surface expression level was tightly matched before comparing the adhesion of two transfectants under flow.

Under flow, a significant effect on adhesion could be detected at all tested shear levels. At 0.7 and 1.8 dynes/cm^2, the rolling flux of LLC (microvillus) was app. 45% of that of LLL (microvillus). This impairment is likely to be caused by the missing cytoplasmic α-actinin binding site that was shown to play a central role in leukocyte tethering under flow (85,128). While truncation of the distal C-terminal part of the intracellular domain responsible for α-actinin binding severely reduces leukocyte tethering via L-Selectin, the microvillus expression pattern is preserved. In contrast, CD44 adhesion does not seem to rely on specific intracellular interactions (129).

Receptor presentation on microvilli is sufficient for increasing adhesion under physiologic shear conditions as shown by LLC compared with LCC (on the cell body, Figure 2.14). These results are further emphasized by reciprocal experiments using CD44 chimeras. Both microvillus-expressed constructs containing the TM domain of L-selectin (CLC, CLL) showed superior adhesion compared with their cell body-expressed counterpart under flow (Figure 2.18) but not under static conditions (Figure 2.12). Thus, the strong enhancement of CD44 adhesion under flow through the introduction of the L-Selectin's TM segment is likely to be a functional consequence of the receptor shift from the cell body to microvilli. Together, these findings emphasize that the TM domain is responsible for specific receptor surface positioning with direct consequences on receptor functionality.

Tight regulation of leukocyte extravasation into tissue is crucial to the homeostasis of the human body. Receptor site densities, structural conformations of receptor complexes and shear conditions are factors constituting avidity while molecular binding kinetics of single bonds describe affinity. Blood consists of about 40-50% of corpuscular elements emphasizing the importance of hemodynamics in cell-endothelium interactions. Capillaries feature a diameter of 5-10 µm and require most cells to deform and squeeze through. This close contact zone, however, gets smaller with increasingly wider post-capillary vessels subjecting the cells to a dispersal force towards the longitudinal axis and away

from the endothelium. Particularly in this high shear environment, the topographic availability on the cell surface has an important impact on cellular adhesion as first shown by von Andrian et al. (75) and further supported in this study. Clustering L-selectin, PSGL-1 and α_4-integrins on microvillus platforms increases avidity and reduces the distance to their ligands. It might also play a role in overcoming electrostatic repulsion between negatively charged particles on both sides.

Notably, technical limitations of a parallel plate flow chamber used in this study impede to mimic exact physiological circumstances such as *in vivo* shear stresses up to 40 dynes/cm^2 (130), flow disturbances caused by erythrocytes and a proper endothelial layer. It is therefore possible that the contributions of microvillus receptor expression to adhesion are even more accentuated.

3.2 Membrane Spanning Domains

In the past few years, functional aspects of membrane spanning domains gained considerable interest (131,132). Next to a general function as membrane anchors, they also play a critical role in receptor functionality. Through lateral membrane interactions or dynamic conformational changes, TM domains are known to regulate the formation of heterogeneous protein complexes and protein folding, yet there is to date no evidence about any particular impact on receptor localization. The T-cell receptor complex uses a network of transmembranal interactions for proper assembly and transport to the cell surface (133). Moreover, the TM segment of the tumor necrosis factor α converting enzyme (TACE) is believed to play a decisive role in regulatory specificity of protein cleavage (134). On the molecular level, the role of the TM domain in cell surface positioning could involve local interactions with other membrane proteins, homotypic assembly or interactions with the lipid bilayer of the surface membrane.

The biological importance is highlighted by several disease-associated mutations within single-spanning TM domains clinically leading to severe pathologies such as achondroplasia, acute myeloid leukemia or lupus (131). Since the extent of microvilli on cancer cells is correlated with the tumor’s potential to disseminate

hematogenously (99), these findings indicate a role of the transmembrane domain of adhesion receptors in metastasis. Insights about the physiology of TM interactions can therefore guide studies into new therapeutic targets in inflammation and cancer metastasis.

3.3 Conclusion and Further Prospects

Taken together, despite a very similar phenotype, the underlying mechanism for the association of different surface receptors with microvilli seems not to be redundant in the first place. Cytoskeletal anchorage as well as extracellular and transmembrane interactions such as lipid raft integrity might be concomitant factors that ultimately contribute to a microvillus expression pattern. However, although both CD44 and L-selectin are genetically and functionally two clearly distinct adhesion receptors, their surface patterns are exclusively directed by interactions in the membrane plane indicating that this might describe a general mechanism. Owing to tight spatial dimensions and dynamics in microvillus morphology, it is also conceivable that some of these processes might be in part dependent on one another.

Further experiments are required to elucidate the importance of the segregation of adhesion receptors involved in leukocyte migration *in vivo*, to reveal specific intramembranous interactions, to investigate vesicular protein trafficking in unpolarized cells and lipid raft integrity in K562 and primary cells.

In conclusion, the insight that transmembrane domains are critical for functions beyond mere anchoring to the lipid bilayer is demonstrated by the striking capability of the membrane spanning domain to compartmentalize surface receptors independent of specific intracellular interactions. This constitutes a novel mechanism of lateral membrane interactions that regulates the functionality of leukocyte adhesion receptors.

4 Materials and Methods

4.1 Chemicals and Cell Culture Substances

- Hyaluronic acid from rooster comb, *Sigma-Aldrich*
- Ampicillin Sodium Salt, *Invitrogen*
- Geneticin liquid 50 mg/ml, *Invitrogen*
- Blasticidin S Hcl, *Invitrogen*
- Penicillin-Streptomycin liquid, *Invitrogen*

4.2 Buffers and Solutions

Western Blot

- TBS: 150 mM NaCl, 10 mM Tris, pH 8.0
- TBST: TBS + 10% Tween20
- Transfer buffer (10x): 30.3 g Tris Base, 144.1 g Glycine, adH_20 1000 ml
- Blocking solution: Dry Milk (5%), Tween20 (0.1%) in Tris Saline

Miscellaneous

- PBS buffer, *Invitrogen*
- HBSS buffer, contains 1.2 mM Ca^{2+}, *Lonza*
- LB-Miller: 2.5 g Yeast Extract, 5 g NaCl, 5 g Tryptone, H_20 500 ml
- Cell sorting buffer: 1x PBS ($Ca^{2+/}Mg^{2+}$ free), 1 mM EDTA, 25 mM HEPES pH 7.0, 1% FBS (heat-inactivated), 0.2 µm filter, sterilize, storage at 4º C

4.3 Commercial Kits

- Miniprep qiaprep spin, *Qiagen*
- Maxiprep qiafilter, *Qiagen*
- Gel extraction kit qiaquick, *Qiagen*
- Nucleofection Kit, *Amaxa*
- Phusion Polymerase PCR kit, *Finnzymes*
- T4 DNA ligation kit, *NEB*

4.4 Eukaryotic Expression Vectors

pcDNA6 V5 HisA

- Promoter: Human CMV
- Primer: 5‘ T7, 3‘ BGH-rev
- Antibiotic resistance: Blasticidin, Ampicillin
- Source: Invitrogen

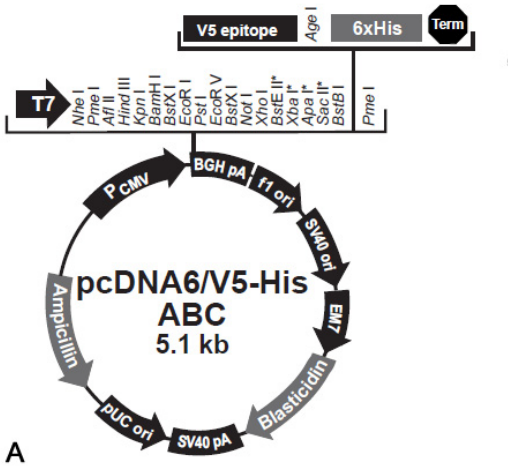

Figure 4.1: (A) pdDNA6 V5 HisA vector map with a multiple cloning site, a CMV promoter and Ampicillin and Blasticidin resistance (Invitrogen). The inserts used feature their own start codon.

4.5 Antibodies

- DREG-56-PE: Mouse anti-human CD62L, conjugated with Phycoerythrin
- DREG-56-FITC: Mouse anti-human CD62L, conjugated with Fluorescein
- Pgp-1-PE: Mouse anti-human CD44 mAb, conjugated with PE
- $IgG_{1\kappa}$-PE: Mouse anti-human $IgG_{1\kappa}$ mAb, conjugated with PE
- Pgp-1: Mouse anti-human CD44 mAb, clone 2C5
- DREG-55: Rabbit anti-human CD62L mAb
- DREG-200: mouse anti-human L-selectin mAb
- Anti-CD44 mAb, clone 515
- Goat anti-rabbit and goat anti-mouse $IgG(F_c)$ conjugated with 10nm gold

All flow cytometry antibodies were purchased from BD Bioscience (San Jose, USA). DREG-55 and DREG-200 were provided by E.C. Butcher (Stanford University, USA). Gold-labeled antibodies were purchased from GE Healthcare. Anti-CD44 mAb clone 515 and clone 2C5 were obtained from R&D Systems.

4.6 Cell Lines and Bacteria

K562

- Human chronic myeloid leukemia in blast crisis
- CD pattern: L-selectin, CD44, LFA-1, Mac-1: negative.
- Double time: 30-40h
- Medium: 90% RPMI 1640 + 10% FBS + 1% Penicillin/Streptomycin
- Subculture: Maintained at 0.1-0.6 × 10^6 cells/ml at 37ºC and 5% CO_2. Passage every 2-3 days. Maximal density at 1.0-1.5 × 10^6 cells/ml to harvest.
- Storage: Frozen 70% medium, 20% FBS, 10% DMSO at -196ºC.
- Source: Deutsche Sammlung von Mikroorganismen und Zellkulturen (DSMZ)

DH5α

- Competent E. coli for subcloning via heat-shock transformation
- Medium: LB-Miller
- Source: Invitrogen

4.7 Restriction Enzymes

- EcoRI: 5‘…G | A A T T C…3‘
- BamHI: 5’…G | G A T C C…3’
- XhoI: 5’…C | T C G A G…3’
- EcoRV: 5’…G A T | A T C…3’
- PST-1: 5’…C T G C A | G…3’
- HINDIII: 5’…A | A G C T T…3’

All restriction enzymes were purchased from NEB.

4.8 Machines and Software

Flow Chamber Setup

- Programmable pump in drawing mode, *harvard apparatus*
- Inverted Microscope Axiovert 100 with the objective 10x 0.25, *Zeiss*
- Microscope modulation contrast, *Hofmann*
- Highspeed Camera sensicam qe, *the cooke cooperation*
- PC precision 690, 2Ghz, 3Gb RAM for video recording, *Dell*
- PC xw4600, 2,66Ghz, 4Gb RAM for data analysis, *Hewlett Packard*
- MatLab2008a for velocity calculations, *The MathWorks Inc.*
- ImageJ software for image analysis, *Available from the NIH*
- CamWare, recording software, *the cooke cooperation*

Miscellaneous

- FACSCalibur for flow cytometry, *BD Pharmingen*
- FACSAria for cell sorting, *BD Pharmingen*
- Cellquest Pro, flow cytometry software, *BD Pharmingen*
- ABI Prism 310 for DNA sequencing, *Perkin Elmer*
- Gel Documentation System, *BioRad*
- NanoDrop 1000, Thermo Scientific
- Inverted microscope Axiovert 25 for cell counting, *Zeiss*
- Tabletop centrifuge 5418, *Eppendorf*
- High speed centrifuge Sorvall Legend RT+, *Thermo Scientific*
- High precision balance, *Mettler AE50*
- Incubator shaker sci I24, *New Brunswick*
- PCR Mastercycler personal, *Eppendorf*

4.9 Bradford Protein Assay

The Bradford protein assay measures the concentration of a protein in a solution based on a spectroscopic shift of Coomassie dye upon binding. The cationic unbound dye is red (470 nm), whereas the bound form turns blue (595 nm). It

essentially binds to cationic and hydrophobic residues, mostly arginine and lysine via van der Waals and ionic interactions.

The standard curve is generated through a BSA dilution series of defined concentration with semi-linear regression of the data points (x-axis log, y-axis linear). Since the ligand PSGL-1 used for adhesion assays was previously self-extracted, its concentration had to be verified. Based on a standard curve, the concentration of PSGL-1 was confirmed to be 1 mg/ml in the given stock solution.

4.10 Recombinant DNA

A polymerase chain reaction (PCR) allows quick *in vitro* amplification of DNA or RNA with a concentration as small as one single molecule based on enzymatic replication. Furthermore, this method can be modified in different ways to insert mutations into the template or to swap domains in a very precise way.

Two flanking oligonucleotides frame the region to be amplified. A buffer solution supplemented with deoxynucleoside triphosphates (dNTPs = dATP, dGTP, dCTP, dTTP) and divalent cations, usually Mg^{2+}, provide an optimized environment for the polymerase. It sets in motion a chain reaction with exponential growth based on repeated temperature changes called thermal cycles.

The first denaturation step at a temperature as high as 98º C melts both complementary DNA strands by disrupting hydrogen bonds. Subsequent lowering to 50-65º C enables the primers to anneal to the single-stranded template. The exact setting depends on the primer design because long oligonucleotides and high cytosine/guanine fractions require higher temperatures. In the third step the polymerase can start the 5' to 3' elongation process by adding dNTPs through condensation of the 5'-phosphate group with the 3'-hydroxyl group. This step's optimum temperature depends on the polymerase, usually ranging between 72 and 78º C. The length of the anticipated fragment needs to be taken into consideration as the extension speed of polymerases can vary. Now this whole cycle is being repeated about 20-30 times whereupon the newly generated fragments now serve as templates again, thus resulting in an exponential yield.

Instead of a three-step cycle, a time-saving two-step cycle combining the annealing and elongation process can be carried out if the annealing temperature is close to the elongation temperature. The final elongation step ensures that every remaining single-stranded template is fully extended and is followed by a 4º C step on hold for short-term storage till further use.

4.10.1 PCR Protocol

All PCRs were carried out in a reaction volume of 50 µl. The sample was prepared on ice. Importantly, the polymerase is the last component to be added. PCR settings and primers for all generated chimeras are indicated in chapters 4.10.4 to 4.10.7.

Table 4.1 Standard PCR protocol

	Volume [µl]	Concentration
Buffer (5×)	10	1×
DNA template	1-5	80-300 ng
dNTPs (10 nM)	1	200 µM
Primer (100 µM)	1	0.5 µM
Phusion polymerase	0.5	0.02 U/µl
H_20	ad to 50	

4.10.2 PCR Optimization

Improving the PCR performance and error rate comprises usage of a suited polymerase, properly designed primers, adjusting cation concentrations, determining the best temperature cycles and avoiding contaminations. This is particularly important in this experimental setup, as no minor aberration of the domain swapped constructs can be tolerated.

The Phusion polymerase by Finnzymes was used due to its high fidelity. It drastically lowers the error rate of amplification steps, being about 50 times more accurate than the Taq polymerase. Therefore, this enzyme is well suited for cloning procedures. The ideal melting temperature T_m can be determined using Finnzyme's T_m calculator for PCR based on Breslauer's thermodynamic

algorithm. With respect to the ideal setting for the duration of the elongation process, a 1 kb DNA fragment is copied within 15 to 30 seconds.

For primers to be efficient, certain requirements ought to be met. Ideal primer design comprises a length ranging preferentially between 18 and 30 nucleotides and a cytosine-guanine content of 40-60%. Furthermore, the melting temperature of both primers used should roughly match, be higher than 60º C but not exceed the polymerase's preferred elongation temperature. Depending on the primer's primary structure, complementary sequences at both ends have the potential to form internal or external secondary structures resulting in a hairpin or primer-dimer conformation, which should be avoided. GC-rich parts located at the 3' part as well as a terminal 5' thymine render the primer more prone to mispriming. For the same reason, sequence elements such as restriction site are to be implemented at the 5'. However, not all rules can usually be respected due to a limited flexibility of primer design.

Contamination is a common source of ineffective and unspecific reactions. Hence, a negative PCR control without DNA was routinely run in parallel.

A too low concentration of free Mg^{2+} reduces the enzyme's activity and might be due to cross reactions with dNTPs, oligonucleotides or contaminating proteins. Determining the optimal amount of divalent cations such as magnesium is therefore critical for a high PCR yield.

Even though ideal melting temperatures can be predicted by software, the individual combination of primers and template often makes adjustments necessary. This can best be achieved by running a gradient on the melting temperature with incremental steps of 0.5º C covering a range of about 3-5º C around the predicted value. A quantitative gel electrophoresis of all samples reveals the best thermal conditions for each reaction.

4.10.3 Domain Swapping

Wildtype L-selectin and CD44 as well as LCL and CLC were already available in the laboratory. The strategy for cloning the missing four L-selectin/CD44 chimeras was based on domain swapping through sequence overlap extension

PCR (135). A pre-existing chimera or wildtype protein served as template in the first polymerase chain reaction. Either the intracellular, the transmembrane or both domains were amplified using a 3' primer that features a splicing site at its 5' end. At the beginning of the amplification process only parts of the primer can anneal properly because the other part is not represented on the template, e.g. the additional restriction site or the artificial DNA extension that functions as linkage to another protein's domain. Only after some PCR cycles will there be enough amplificated DNA that then allows the primers to anneal completely. This distinction is important inasmuch as the melting temperatures change. Thus, the PCR settings for the first few and the subsequent steps are different. The resulting small DNA fragment consisting of one or two protein domains linked to a restriction site is detected and isolated by gel electrophoresis and a gel extraction kit. The concentration of a 20 µl elution was usually as low as some ng/ml, yet enough to conduct the second PCR reaction. Now the isolated DNA fragment serves as reverse primer which is rather long compared to the forward primer. For this reason, the melting temperatures of both primers differ markedly. The second PCR provides the anticipated protein chimera linked to a defined restriction sites.

For the protein's proper integration into the vector, the insert needs to be extended with appropriate restriction sites at both ends. Both sites were chosen with respect to the multiple cloning site of the vector pcDNA6. BamHI and HINDIII restriction sites allowed all inserts to be specifically integrated into the vector. These restriction enzymes, both of which lead to a sticky DNA extension (chapter 4.7), were verified to cleave both the vector and the insert uniquely at one single location. As restriction enzymes cleave DNA much less efficiently towards the end of a fragment, an additional 5' extension of 2 to 10 nucleotides enhances the cleavage efficiency of most enzymes. All inserts provide their own start codon so that a possible frame shift upon religation does not have to be taken into account.

4.10.4 Chimera: LCC

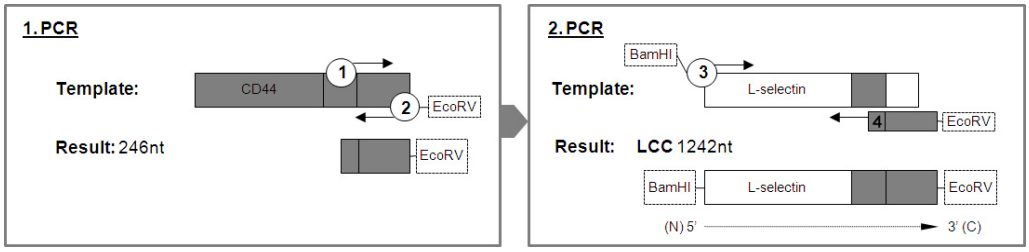

Primers

Number	Primer name	nt	%CG	T_m	Sequence 5' → 3'
1	tmCD44_fwd	23	48	69.1	GCAGT TTGCA TTGCA GTCAA CAG
2	icCD44_EcoRV_rev	22 31	45 39	64.9 69.6	TTACA CCCCA ATCTT CATGT CC AAAGA TATCT TACAC CCCAA TCTTC ATGTC C
3	LSel_BamHI Kozakmut_fwd	25 33	45 49	64.9 80.8	GCCAT GGTGT TTCCA TGGAA ATGTC AAGGA TCCGC CATGG TGTTT CCATG GAAAT GTC
4	PCR product	22 246	41	63.9 > 90	

PCR Protocol

Step		1.PCR		2.PCR	
Initial denaturation		98°C 30s		98°C 30s	
First cycle	Denaturation Annealing Elongation	98°C 10s 68°C 30s 72°C 15s	Repeat 5 times	98°C 10s 67°C 30s 72°C 30s	Repeat 5 times
Second cycle	Denaturation Annealing Elongation	98°C 10s 72°C 15s	Repeat 25 times	98°C 10s 72°C 30s	Repeat 25 times
Final elongation		72°C 5min		72°C 5min	
Final hold		4°C		4°C	

4.10.5 Chimera: CLL

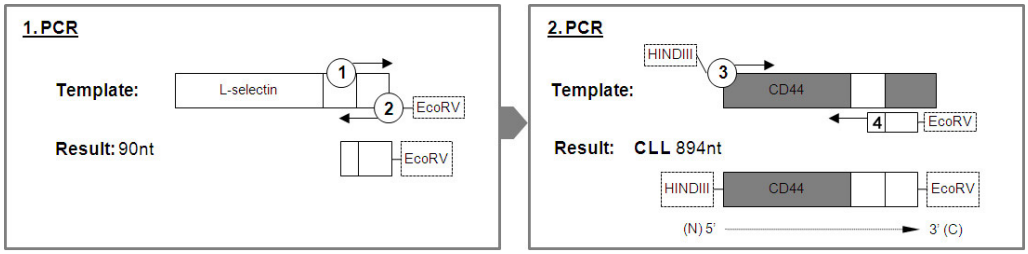

Primers

Number	Primer name	nt	%CG	T_m	Sequence 5' → 3'
1	tmLSel_fwd	24	46	70.6	GGGTT GGCAT TTATC ATTTG GCTG
2	icLSel_EcoRV_rev	23 32	31 28	56.7 63.4	TTAAT ATGGG TCATT CATAC TTC AAAGA TATCT TAATA TGGGT CATTC ATACT TC
3	CD44_HindIII_fwd	18 33	44 46	58.8 78.6	ATGGA CAAGT TTTGG TGG TTTAA GCTTG CCACC ATGGA CAAGT TTTGG TGG
4	PCR product	18 90	38	58.0 > 90	

PCR Protocol

Step		1.PCR		2.PCR	
Initial denaturation		98ºC 30s		98ºC 30s	
First cycle	Denaturation Annealing Elongation	98ºC 10s 60ºC 30s 72ºC 15s	Repeat 5 times	98ºC 10s 58ºC 20s 72ºC 30s	Repeat 5 times
Second cycle	Denaturation Annealing Elongation	98ºC 10s 67ºC 30s 72ºC 15s	Repeat 25 times	98ºC 10s 67 ºC 20s 72ºC 15s	Repeat 25 times
Final elongation		72ºC 5min		72ºC 5min	
Final hold		4ºC		4ºC	

4.10.6 Chimera: LLC

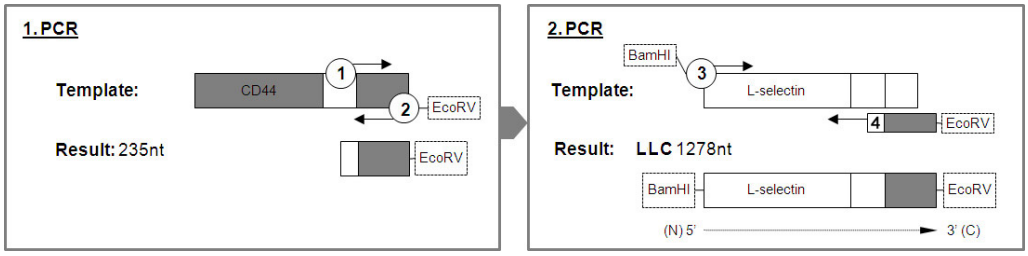

Primers

Number	Primer name	nt	%CG	T_m	Sequence 5' → 3'
1	tmSel_icCD44_fwd	43	51	86.0	GGCAT TTATC ATTTG GCTGG CACGA AGAAG GTGTG GGCAG AAG
2	icCD44_EcoRV_rev	22 31	45 39	64.9 69.6	TTACA CCCCA ATCTT CATGT CC AAAGA TATCT TACAC CCCAA TCTTC ATGTC C
3	LSel_BamHI Kozakmut_fwd	22 33	45 49	64.9 80.8	ATGGT GTTTC CATGG AAATG TC AAGGA TCCGC CATGG TGTTT CCATG GAAAT GTC
4	PCR product	22 235	45	69.7 > 90	

PCR Protocol

Step		1.PCR		2.PCR	
Initial denaturation		98ºC 30s		98ºC 30s	
First cycle	Denaturation Annealing Elongation	98ºC 10s 68ºC 20s 72ºC 15s	Repeat 5 times	98ºC 10s 59ºC 30s 72ºC 30s	Repeat 5 times
Second cycle	Denaturation Annealing Elongation	98ºC 10s 72ºC 20s	Repeat 25 times	98ºC 10s 72ºC 30s	Repeat 25 times
Final elongation		72ºC 5min		72ºC 5min	
Final hold		4ºC		4ºC	

4.10.7 Chimera: CCL

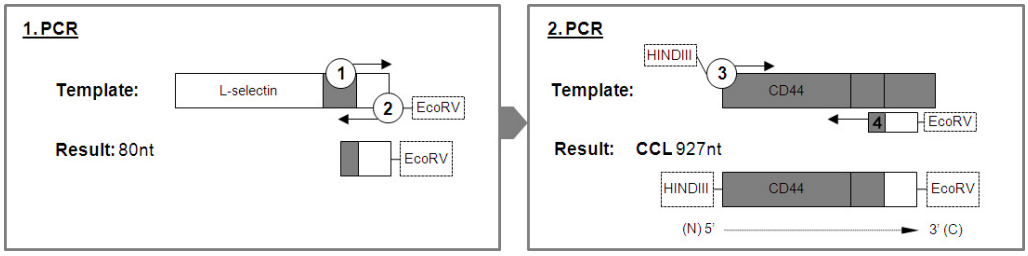

Primers

Number	Primer name	nt	%CG	T_m	Sequence 5' → 3'
1	tmCD44_icSel_fwd	34	38	72.3	GCATT GCAGT CAACA GTAGG AGATT AAAAA AAGG
2	icSel_EcoRV_rev	23 32	46 28	56.7 68.4	TTAAT ATGGG TCATT CATAC TTC AAAGA TATCT TAATA TGGGT CATTC ATACT TC
3	CD44_HindIII_fwd	18 33	43 46	58.8 78.6	ATGGA CAAGT TTTGG TGG TTTAA GCTTG CCACC ATGGA CAAGT TTTGG TGG
4	PCR product	17 80	74	55.9 > 90	

PCR Protocol

Step		1.PCR		2.PCR	
Initial denaturation		98ºC 30s		98ºC 30s	
First cycle	Denaturation Annealing Elongation	98ºC 10s 57ºC 20s 72ºC 15s	Repeat 5 times	98ºC 10s 60ºC 30s 72ºC 30s	Repeat 5 times
Second cycle	Denaturation Annealing Elongation	98ºC 10s 67ºC 20s 72ºC 20s	Repeat 25 times	98ºC 10s 72ºC 30s	Repeat 25 times
Final elongation		72ºC 5min		72ºC 5min	
Final hold		4ºC		4ºC	

4.10.8 Plasmid DNA Purification

DNA was isolated out of transformed bacteria using the Qiagen plasmid purification kits. Depending on the amount of DNA to be recovered, the small (< 40 µg), midi (< 400 µg) or maxi (>400 µg) kit was used according to the manufacturer's instructions.

After transformation and overnight culture, the bacteria are lysed through an alkaline lysis method. The lysate is then neutralized and adjusted to high-salt binding conditions. A silica membrane column ensures a selective absorption of DNA, whereas RNA, endonucleases, proteins and other metabolites are eliminated by several washing steps. The subsequent elution is based on a low-salt filtration. The DNA yield and pureness can be measured either by gel electrophoresis with a quantitative mass standard for low yield purifications or by photometry at 260 nm.

4.10.9 DNA Gel Electrophoresis

Gel electrophoresis is a means to separate DNA, RNA or proteins using an electric current applied to the gel matrix. The gel consists of a crosslinked polymer whose porosity accounts for the speed of the molecules migrating through the gel matrix. The movement is furthermore determined by the molecule's mass to charge ratio and makes the negatively charged DNA move towards the anode. Agarose is the preferred matrix composition for DNA separation. For visualization of the DNA bands, the intercalating agent ethidium bromide can be used. It serves as a fluorescent tag when exposed to ultraviolet light. This method can be employed for both analytical and preparative purposes.

DNA gel electrophoresis was performed either for the identification of successfully cloned protein chimeras after specific digestion or for isolating a certain DNA fragment out of the PCR sample for further experiments. 2 µl 6× loading buffer was added to 10 µl sample volume. A 0.7% or 1.5% agarose gel was used for fragments bigger or smaller than 500 bp, respectively, and run at 90 V for approximately one hour. Depending on the expected fragment size, the 1 kb

or 100 bp mass standard served for sizing. Pictures of the stained gel were acquired by a gel documentation system.

4.10.10 DNA Gel Extraction

The DNA gel extraction kit from Qiagen uses the principle of an anion exchanger to separate the gel matrix from the DNA with subsequent elution by water. The desired gel band was cut out and dissolved in an adequate volume of QB-buffer for 10 min at 50° C. The suspension was then centrifuged using a centrifugation column with silica membrane that binds DNA in a high salt buffer. Two washing steps remove primers, nucleotides, enzymes, salts, agarose and ethidium bromide. The purified DNA was then eluted using a low-salt buffer. All centrifugation steps were carried out at 10.000 g for 1 min at room temperature.

4.10.11 Ligation

The ligation process describes the synthesis of a new phosphodiester bond between a vector backbone and a DNA strand to be inserted. For all ligation purposes, the T4-DNA-ligase with an appropriate buffer was used.

Table 4.2 Standard protocol for DNA ligation.

Digested vector (0.5 ng/µl)	2-4 µl
Insert	1-6 µl
T4 ligase (2 U/ µl)	1 µl
T4 buffer (10×)	1 µl
H_20	ad to 10 µl

Importantly, the ratio between the vector and the insert was aimed to be 1:3 as measured by a gel electrophoresis (comparison of band intensities). All samples prepared according to Table 4.2 were incubated for at least 2 h at room temperature before the transformation into DH5α bacteria.

Several controls ensured the quality of the cloning process:

- A double digested vector was transformed without ligation indicating the effectiveness of the double digestion.

- A double digested vector was ligated and transformed revealing unspecific religation processes.
- A single digested vector was ligated and transformed as a positive control proving the T4 ligase enzyme activity.

4.10.12 Transformation

The ligation samples were transformed into competent DH5α bacteria via heat-shock-transformation. Briefly, the ligation sample was added to 50 µl of competent E.coli bacteria and incubated on ice for 20 min. After the heat-shock at 42° C for 70 s, the cells were immediately put on ice for another 10 min. 300 µl pure LB-medium was added to the cells which then were incubated at 37° C on a shaking platform for 30 min. This sample was eventually plated on antibiotic containing agar plates overnight at 37° C.

4.10.13 Sequencing

The base sequence of all cloned constructs was verified by DNA sequencing using the chain-terminator method by F. Sanger. A single stranded DNA template is replicated by the DNA polymerase starting at the given primer. Apart from physiologic desoxynucleotide triphosphates (dATP, dGTP, dTTP, dCTP), there are also a didesoxynucleotide triphosphates (ddNTPs) as DNA chain terminators supplied in the reaction buffer. In contrast to dNTPs, they lack the 3'-OH group required for the formation of the phosphodiester bond and are fluorescently labeled. Both are equally handled by the polymerase resulting in a random termination of the elongation process and thus DNA fragments of varying length. The pattern of a gel electrophoresis with analysis of the fluorescent dyes can be eventually translated into a DNA sequence.

A sequencing kit and the sequencer ABI Prism 310 by Perkin Elmer was used according to the manufacturer's instructions.

After the PCR (96°C, 1min; (96° C, 10 s; 50° C, 5 s; 60° C, 4 min) repeat 25 cycles; 15° C, ∞), the sample was transferred to dehydrated DyeEx-columns and centrifuged. A subsequent vacuum centrifuge step for 5 min evaporated the

solvent and the remaining DNA was resolved in 20 µl template suppression reagent for 3 min at 96° C. The sample was then analyzed by the sequencing machine.

Table 4.3 Standard protocol for DNA sequencing.

Plasmid	1 µl
Primer (10 µM)	0.5 µl
BDT v1.1 (kit)	0.25 µl
Buffer (5 ×)	2 µl
H_20	ad 10 µl

4.11 Cell Transfection and Culture

Eukaryotic cell transfection using the Amaxa nucleofection kit was performed according to the manufacturer's instructions. K562 cells were passaged two days before transfection to obtain a cell density of 2-5 × 10^6 cells/ml. Since the procedure affects cell vitality, all steps need to be carried out quickly. Required materials:

- 37º C prewarmed RPMI 1640 medium + 10% FCS
- 6 or 12 well plate, each needed well with 1500 µl prewarmed medium
- Nucleofection factor at room temperature (comes with the Amaxa kit).
- 1 × 10^6 cells spinned down at 300 g for 5 min.
- Highly purified vector DNA, 2 µg per reaction needed.
- Amaxa electroporation device, sterile cuvettes and sterile plastic pipettes.

One nucleofection sample contained 1 × 10^6 cells resuspended in 100 µl nucleofection factor. After adding 2 µg DNA (in 1 to 5 µl), the suspension was transferred into the sterile cuvette and electroporated using the right predefined setting for the cell type used (e.g. T-16 for K562 cells). 500 µl prewarmed medium was immediately added to the cuvette and then gently transferred to the well plate with a sterile plastic pipette.

A GFP-vector served as a positive control, a sample without DNA as negative control. After incubating the transfected cells for 2 days, they were passaged this

time using a medium with eukaryotic antibiotics to start the positive selection process.

The human chronic myeloid cell line K562 was grown in RPMI 1640 medium supplemented with 10% fetal bovine serum and 1% penicillin/streptomycin at 37º C and 5% CO_2. Cells were passaged every 3-4 days to a density of 1-2 × 10^5 cells/ml. Higher densities than 1.5 × 10^6 cells/ml and lower than 0.1 × 10^6 cells/ml were avoided.

Cell vitality was assessed on a regular basis by trypan blue staining and it constantly showed a viability greater than 90%. A 1:10 dilution in PBS of the dye was mixed with cells 1:1 and then counted on a hemocytometer. Viable cells don't take up the dye and won't be stained blue. Because of trypan toxicity the sample was analyzed not later than 30 minutes after staining.

4.12 Immunoblot

Immunoblot (Western Blot) is an analytical method for the quantitative detection of specific proteins in a tissue or cell homogenate. First, the cells are sonicated to break up their integrity and render their components accessible for further treatment. Using gel electrophoresis the sample suspension is subsequently separated by the length of its polypeptides. The most common technique is the 2D SDS-PAGE using a polyacrylamide gel and sodium dodecylsulfate (SDS) as a detergent. SDS denatures proteins by reducing disulfide linkages and uniformly covers the target molecule with a negative charge. The separation process is therefore entirely dependent on the polypeptide's length and the gel's porosity and does not take other effects into account such as individual charge, tertiary protein folding or quaternary structure. The protein pattern is then moved onto a nitrocellulose membrane by a tank blot assay. It is followed by a two step immunostaining process with a primary antibody against the desired epitope and a secondary antibody most commonly conjugated with the horseradish peroxidase (HRP). In conjunction with a chemiluminescent substrate the reaction produces luminescence directly proportional to the amount of protein. A photographic film is eventually exposed to the light creating a pattern of detected proteins bound to the blot.

In this project, western blot analysis with surfaced expression matched transfectants was conducted to show the total amount of expressed protein within the cell, thus revealing protein trafficking issues of the different chimeras. A control stained for the cytosceletal ß-actin ensured quantitative consistency of all loaded samples.

Protocol

- Collect 2 × 10^6 cells, wash twice in PBS and dissolve in 500 µl PBS
- Add 5 µl 100x PIC (protease inhibitor cocktail)
- Sonicate 12 x, put on ice immediately.
- Add 50 µl ß-mercaptoethanol to 950 µl Laemmli buffer and preheat 500 µl 5 min at 95º C
- Add 500 µl buffer to cell suspension (2 × 10^6 cells in 1 ml)
- Incubate 10 min at 95º C (hereafter samples can be freezed down)
- Load 7.5% gel with 5 µl marker and 10 µl sample (equals 2 × 10^4 cells)
- Run gel at 80 V for 20 min, then 130 V for 30 min
- Prepare blot sandwich (negative to positive):
  sponge, 2 filters, gel, nitrocellulose, 2 filters, sponge
- Run blot at 350 mA for 1h
- Cut the membrane right above 50 kDa to separate ß-actin and the desired protein. Parts can now be treated individually to avoid antibody crossreactions.
- Transfer membrane in 15 ml blocking solution and shake for 60 min at RT.
- Renew blocking solution and add primary antibody overnight at 4º C at the concentration of 1 µg/ml. ß-actin loading control 1:5000 dilution.
- Rinse membrane twice with 10 ml TBST, then wash three times for 10 min in 30 ml TBST.
- Add secondary antibody (horse radish peroxidase conjugated) in a 1:5000 dilution. Shake for 60 min at RT.
- Rinse membrane twice with 10 ml TBST, then wash three times for 10 min in 30 ml TBST.

- Detection of proteins using the ECL kit: Mix solutions A and B as 40:1. Apply on membrane with protein-side up. Incubate for 5 min at room temperature, drain off excess.
- Place membrane in an X-ray cassette. Adjust exposure time.

4.13 Reverse transcriptase PCR

The reverse transcriptase (RT)-PCR is applied to detect the mRNA of transcribed proteins in the transfected cell line K562. It also allows the identification of transfectants that only differ in their transmembrane domain (e.g. LLL and LCL) using a third specific primer (chapter 2.1.2). The Qiagen *One Step RT-PCR kit* was used as follows:

Table 4.4 Standard protocol for RT-PCR

mRNA	100 ng
Primer forward (10 µM)	1 µl
Primer reverse (10 µM)	1 µl
dNTP (10 nM)	2 µl
RT-PCR Buffer (5 ×)	10 µl
Enzyme mix (kit)	2 µl
H_20	ad 50 µl

Forward and reverse primers of L-selectin and CD44 are indicated in chapter 4.10. The PCR was performed at 50° C 30 min, 95° C 15 min, (95° C 30 s, 60° C 30 s, 72° C 60 s) × 40 cycles, 60° C 30 s, 72° C 10 min, 4° C ∞. A gel electrophoresis showed the amplified DNA.

4.14 Flow Cytometry and Cell Sorting

One of the fundamentals of flow cytometry is the ability to measure properties of individual particles. Most common usage is the detection of fluorescently labeled cells or beads that are then quantitatively and qualitatively analyzed with appropriate flow cytometry software.

The fluidic system first manages the injected particles' random distribution in three-dimensional space to be ordered into a single stream. The main core through which the sample is injected is enclosed by an outer sheath that contains faster running sheath fluid. The resulting drag effect on the central chamber creates a single file of particles. This process is called hydrodynamic focusing. Now each single particle passes through beams of light that determine its unique attributes. Light scattered in the forward direction (FSC) roughly specifies the particle's size and allows the distinction between living cells and debris. The side scatter channel (SSC) provides information about the granular content within a particle. Both FSC and SSC in combination may be used to differentiate different cell types in a heterogeneous sample such as whole blood.

Staining cell epitopes with one or multiple fluorescent labeled antibodies provides an additional powerful tool. These fluorochromes are basically dyes that absorb light energy and re-emit it at a longer wave length which can be specifically detected by photomultiplier tubes. Up to 16 or more dyes can be used simultaneously for detecting the expression level of a surface receptor or intracellular molecule, depending on the machine configuration.

4.14.1 Staining Protocol

One unstained sample of cells serves for adjusting the forward and sideward scatter and zeroing the fluorescent channels. An isotype stained sample represents the negative control showing the specificity of antibody binding.

All centrifugation steps were carried out at 300g for 5 min. Samples permanently were kept on ice because repeated changes in temperature may cause activation of cells with consecutive shedding and redistribution of L-selectin.

- Resuspend 1 × 10^6 cells in ice-cold blocking buffer (PBS + 5% FCS).
- Wash two times (spin down, suck off supernatant, add 2-3 ml buffer, vortex).
- Resuspend in 200 µl blocking buffer and add 20 µl fluorescent labeled antibody (1:10 dilution for most BD Pharmingen Antibodies). Incubate 30 min on ice covered from light.

- Dilute antibody concentration by adding 2-3 ml blocking buffer, spin down.
- Wash twice
- Resuspend cells in 300-500 µl buffer for immediate analysis. For permanent storage use 2% glutaraldehyde. Cover from light.

4.14.2 Antibody Titration

For assessment of the binding characteristics of the DREG-56 monoclonal antibody to the lectin domain, a flow cytometry analysis was performed as described above. mAbs were serially diluted to 0.3, 1.5, 3.05, 6.1 and 10.0 µg/ml in PBS. Mean fluorescent intensities (MFI) were determined.

4.14.3 Electrostatic Cell Sorting

A major application for flow cytometry is to separate cells according to subtype or epitope expression for further studies. This process is called cell sorting or fluorescence activated cell sorting (FACS).

Unlike usual flow cytometry analysis, cell sorting requires technically a different set up. After reading the cell's emission wavelength and intensity, the signal is compared to the given selection criteria on the instrument. If it matches, the cell sorter directs the particle into a certain collection tube according to the configuration. This happens by charging the particle-containing drop as it exits the vibrating nozzle of the fluidics system. The droplets then eventually pass through an electrostatic field and are deflected towards the collection tube.

Since the pH regulation of culture media fails under normal atmosphere causing the media to become basic and calcium chloride is precipitates with the phosphate of the instruments sheath buffer, a specific sorting buffer helps optimizing for enhanced cell viability and recovery (chapter 4.2).

Certain factors such as sorting efficiency of the machine, tightness of the sorting gate and time factors lower the outcome of sorted cells. Therefore, a large total number of cells (10-15 × 10^6) needs to be prepared in order to get a sufficient amount of sorted cells to culture. Cells were stained in 1 ml PBS-buffer using a 1:10 antibody dilution. Depending on the transfection quality of the chimeras, the

outcome used to be 0.2 – 1 × 10^6 cells (2-10%). A typical configuration for transfected K562 cells is shown in Figure 4.2. A FSC/SSC diagram allows the selection of the main living cell population. This population is further screened for doublets in a FSC/FSC and SSC/SSC diagram in order to exclude them from the sorting process. The L-selectin expression of the remaining cells (85.5% of all cells) is then visualized in a histogram. Three gates for low (8.4%), medium (20.8%) and high expression (13.0%) fractions were then defined and the sorting was started.

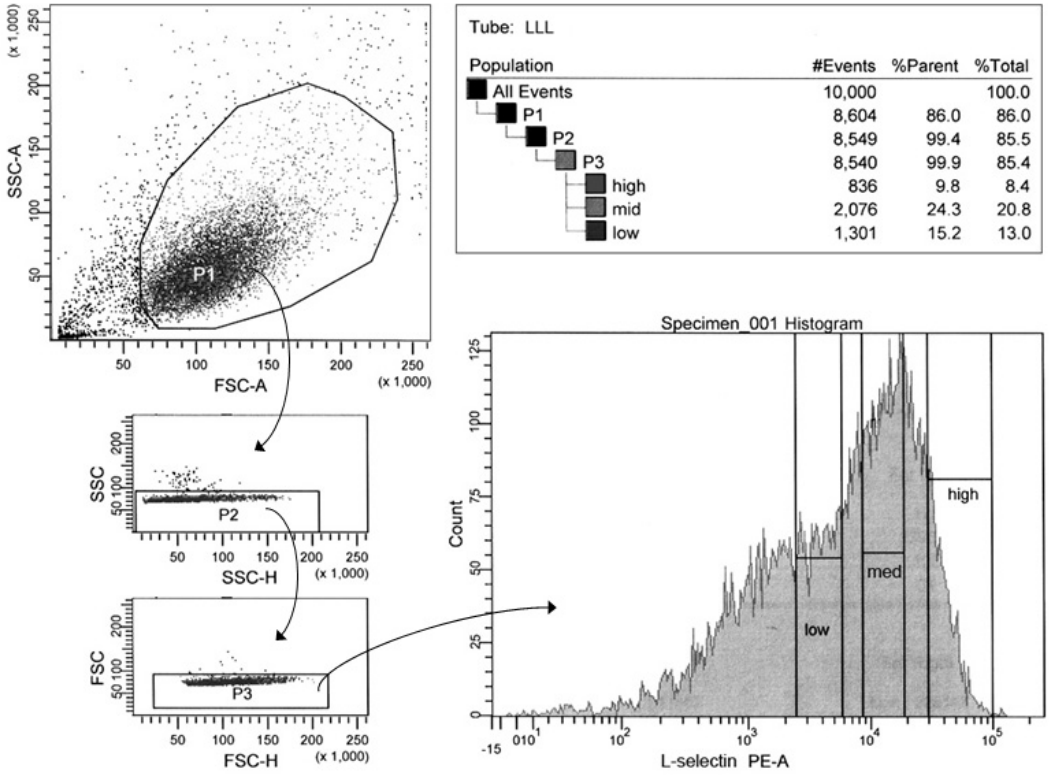

Figure 4.2: Typical cell sorting setup for transfected K562 cells. First, the main population is gated for viable cells, leaving 86.0% in gate P1. A SSC/SSC and FSC/FSC analysis identifies doublets which are entirely sorted out in P3. Three tight gates low, med and high are then applied resulting in three sorted populations with different expression levels.

4.15 Immunoelectron Microscopy

Localization of the L-selectin and CD44 chimeras on transfected K562 cells was examined using a pre-embedding immunolabeling technique as described previously (109). Briefly, 2 × 10^6 cells were incubated with the primary antibody at a dilution of 1:10 in PBS + 1% FCS at 4º C for 10 min. After washing, the

secondary antibody conjugated to 10nm gold particles was added at a dilution of 1:30 for 10 min at 4º C followed by fixation (Karnovsky's fixative) and dehydration. Thin sections were cut on a Reichert Ultracut microtome and stained with 2% uranyl acetate and 2% lead citrate. Images were taken using a Zeiss EM10 microscope.

Microvilli were defined as surface protrusions extending at least 50 nm from the smooth spherical shape of the cell body in agreement to (39). Importantly, the two dimensional images of TEM do not allow differentiation between sheet-like projections (e.g. ruffles or folds) and microvilli. Analysis of the 10 nm colloidal gold distribution was performed by two independent blinded observers at a magnification of 30.000 – 60.000×. For each transfectant, 20-30 cells were analyzed with a total of 700-1400 particles. A mock transfectant as negative control did not show any staining. All electron micrographs were recorded by Prof. Dr. Shakibaei, Department of Anatomy, Ludwig-Maximilians University Munich, Germany.

4.16 Static Adhesion Assay

Hydrophobic glass slides were coated with 2 mg/ml hyaluronan or 30 µg/ml PSGL-1 in PBS and blocked with BSA. 10ml cell suspension (5×10^6 cells/ml, HBSS medium for L-selectin, RPMI 1640 for CD44) was added and incubated at 37º C for 15 min. The amount of adhesive cells was assessed with an inverted microscope Zeiss Axio 100. Cells preincubated with 10 µg/ml blocking mAb (anti-CD44 clone 515 and anti-L-selectin DREG-56) for 10 min at 37º C were used as controls.

4.17 Adhesion Assays under Flow

Due to the complexity of the microcirculation, leukocyte rolling *in vivo* is constantly subject to a variety of changes of hemodynamic and geometric parameters such as vessel size, wall shear stress, flow rate, flow turbulence and hematocrit. Moreover, the endothelial cell layer encircling the vessel lumen hosts a dynamic pattern of adhesion molecules at variable site densities (21).

To address the question of individual substrate ligand binding characteristics, adhesion assays under flow have been developed. They provide a means to mimic *in vivo* hemodynamics *in vitro* under clearly defined flow conditions, thus breaking down the physiological complexity to a more accessible model. A laminar flow system that visualizes adhesive interactions of blood cells and cell lines on a concentrated substrate with defined shear stress conditions is called flow chamber.

Adhesion under flow was investigated using a parallel plate flow chamber from GlycoTech (Gaithersburg, USA) placed on a 35 mm polystyrene dish and connected to a high precision perfusion pump (Harvard Apparatus, Holliston, USA). An inverted microscope Axio 100 (Zeiss, Jena, Germany) was used at 10× magnification equipped with the digital high performance camera SensiCam QE (The Cooke Cooperation, Romulus, USA). As specificity control, cells were incubated for 10 min at 37º C with 10 µg/ml blocking antibody (anti-CD44 clone 515 and anti-L-selectin DREG-56) prior to the experiment.

4.17.1 Parallel Plate Flow Chamber

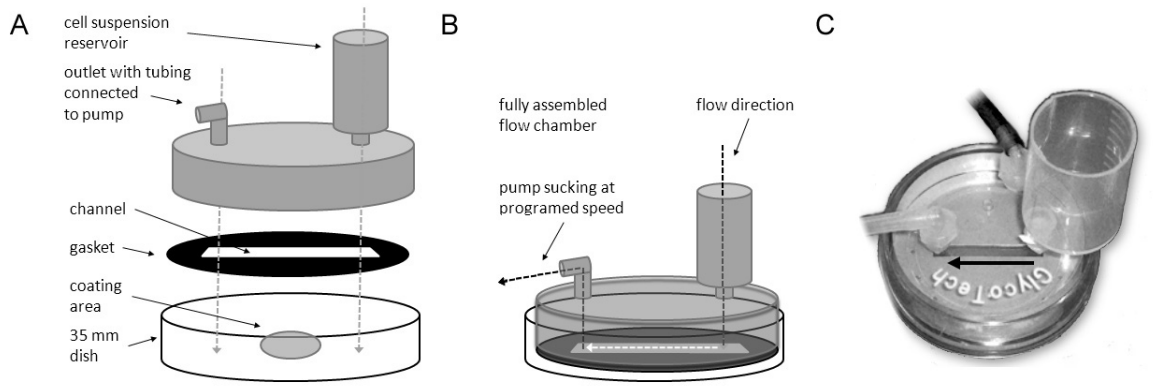

Figure 4.3: Glycotech flow chamber assembly. (A) and (B) Schematic view of the different components. First, a plastic cell culture dish is coated with a certain ligand. Right prior to the experiment, the gasket is attached to the chamber's body which is then placed into the dish. A vacuum suction keeps all components together (not shown in the figure). Second, the cell suspension reservoir is mounted and the distal tubing installed. The cells are perfused through the flow chamber by means of a high precision perfusion pump at the distal end. Flow direction is indicated by arrows as visualized on (B). (C) Working parallel plate flow chamber from Glycotech.

A fully assembled parallel plate flow chamber from GlycoTech is shown in Figure 4.3. It consists of two parallel plates separated by a gasket that forms a channel

between an inflow and an outflow port. Preliminary data revealed the gasket width of 0.25 cm and channel length of 2 cm to be best suitable. For every experiment the gasket and the chamber itself were thoroughly cleaned with 100% ethanol. The cell suspension reservoir was made of a 10 ml plastic syringe cut in half and attached to the flow chamber by a screw lock with sealing band. The reservoir and the 35 mm cell culture dish are disposable and to be used fresh every time. The cell reservoir was directly mounted on the chamber. It minimizes disturbing effects on the cells prior to data acquisition in the channel.

Cells were introduced into the coated channel at a constant velocity defining the shear stress conditions (chapter 4.17.2). Interactions were made visible through an inverted microscope at a magnification of 10×. While non-interacting cells became visible as fast streaks, rolling cells were clearly distinguishable by their reduced velocity (Figure 4.4). Adhesive interactions were made visible through an inverted microscope, focusing on the mid-section of the channel. All data was recorded at 10× magnification with the digital high performance camera SensiCam QE.

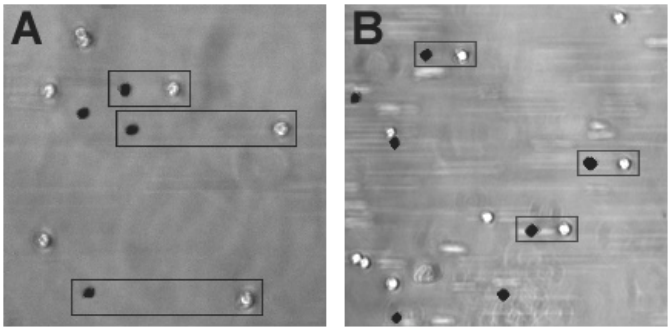

Figure 4.4: White and black circles represent rolling K562 transfectants on a specific ligand at two different time points. Framed pair of cells represents a rolling cell. Free flowing cells become visible as dim streaks. Flow direction from right to left. 10× magnification. (A) LLL on PSGL-1 at 1.3 dynes/cm^2. Time frame shows 1s. (B) CCC on hyaluronan at 0.7 dynes/cm^2 . Time frame shows 2 min.

4.17.2 Flow Dynamics

By means of an automated pump, cells are forced through the channel based on a linear pressure gradient. When freely flowing particles get in contact to a static layer, a shear force applies parallel. This stress affects circulating leukocytes

communicating with the endothelium. The mathematical model to calculate the resulting shear stress on the cells assumes a Newtonian fluid and an infinitely wide distance between the parallel plates of the flow chamber. A fluid is considered Newtonian if the stress-strain curve is linear and therefore incompressible. Importantly, these two conditions are not met *in vivo* as blood is a heterogeneous suspension and the flow chamber has limited dimensions. The wall shear stress τ_w in such a hypothetical steady flow system is determined as a function of the flow and the channel's size (Equation 2). The linear relationship between the wall shear stress and the perfusion rate in a flow chamber is shown in Figure 4.5.

$$\tau_w = \frac{3 * \mu * Q}{2 * b * a^2}$$

Equation 2 Wall shear stress τ_w in a rectangular tube. μ = fluid viscosity, a = channel half height, b = channel width and Q = perfusion rate.

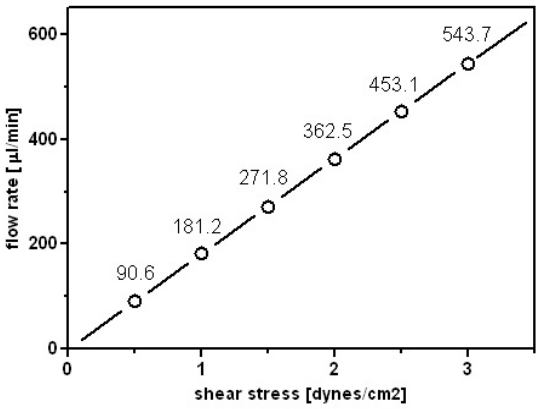

Figure 4.5 Shear stress and flow rate. This curve describes the linear relationship between the shear stress and the flow rate in a parallel plate flow chamber from GlycoTech using a 0.25 cm gasket. Calculated with

Equation **2** (channel length = 2 cm and channel height = 0.25 cm).

A parabolic velocity profile between the plates that vanishes at the boundaries of the channel is a typical attribute of finite parallel flow chamber dimensions (Figure 4.6). Accordingly, the maximum magnitude of the wall shear stress can be found

at the chamber's central surface decreasing to both sides with a complete abolishment in the corners (

Figure 4.7). These parameters are closely related to the chamber's dimensions. The narrower the chamber, the smaller the area that has a homogeneous shear stress profile. It is therefore important to choose the microscopic field of view correctly and to keep it constant in different investigations.

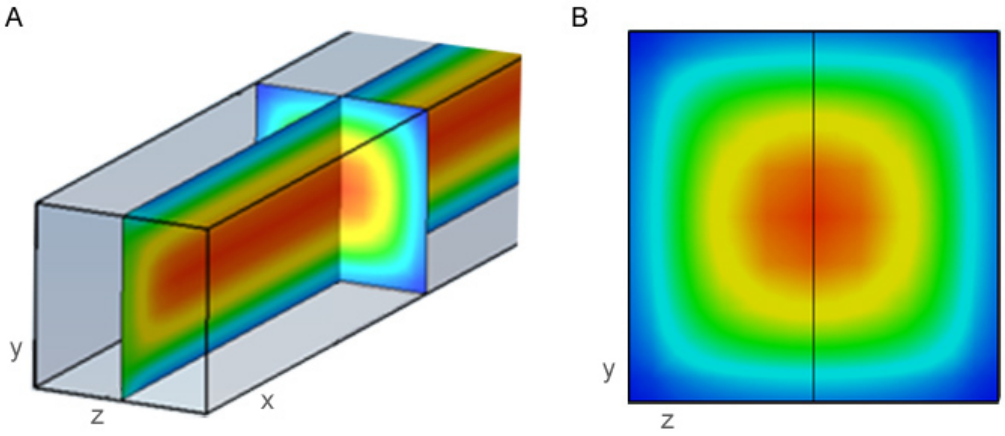

Figure 4.6 Velocity profile in a parallel plate flow chamber. (A) Laminar Flow along the x-axis in a rectangular channel. (B) The cross section highlights the formation of circular streams with the highest velocities in the channel center. Decreasing values from red → yellow → green → light blue → dark blue. Data calculated with Flow Works.

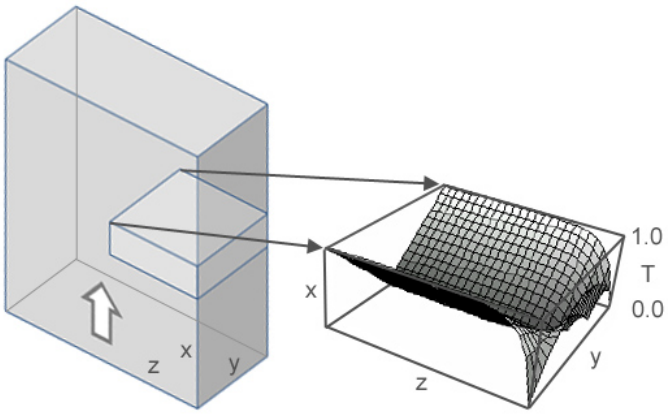

Figure 4.7 Shear stress in a parallel plate flow chamber. A linear pressure gradient forces fluid along the x-axis. The calculated shear stress (T) shows that the values are highest at both parallel plates, somewhat lower at the side borders and vanish in the corners. Arbitrary units. Adapted from **(136).**

4.17.3 L-selectin Rolling on PSGL-1

Each dish was coated with 150 µg/ml recombinant PSGL-1-F_c in PBS for 2 h and then blocked with 2 mg/ml BSA in PBS for 1h. Cells were resuspended in HBSS containing 1.26 mM Ca^{2+} (Lonza, Basel, Switzerland) with a final density of 1×10^6 cells/ml. Rolling assays were started at 2.3 dynes/cm^2 and shear stress was gradually decreased to 1.7, 1.3 and 0.7 dynes/cm^2. Three different fields of view were recorded for a duration of 20 s and extrapolated to 1 min. Velocity determination was performed using a MATLAB (Version 7.5.0, R2007B) cell tracking software by John Pickard (snake model tracking algorithm).

4.17.4 CD44 Adhesion on Hyaluronan

Soluble hyaluronan was plated at 2.0 mg/ml in PBS, incubated overnight at 37º C and subsequently blocked with 2 mg/ml BSA in PBS for 1h. Cells (1×10^6/ml) were washed and resuspended in RPMI 1640 medium. After 7 minutes of flow, pictures of three different fields of view were taken.

5 Summary

During inflammation and immune surveillance, initial contacts (tethering) between free-flowing leukocytes and the endothelium are vitally dependent on the presentation of the adhesion receptor L-selectin on leukocyte microvilli. Determinants that regulate receptor targeting to microvilli are, however, largely elusive. Therefore, we systematically swapped the extracellular (EC), transmembrane (TM) and intracellular (IC) domains of L-selectin and CD44, a hyaluronan receptor expressed on the cell body and excluded from microvilli. Electron microscopy of transfected human myeloid K562 cells showed that the highly conserved TM domains are responsible for surface positioning. The TM segment of L-selectin forced chimeric molecules to microvilli and the CD44 TM domain evoked expression on the cell body, while the IC and EC domains hardly influenced surface localization. Transfectants with microvillus-based chimeras showed a significantly higher adhesion rate to a physiological ligand under flow but not under static conditions as compared to cells with cell body-expressed receptors. Substitution of the IC domain of L-selectin by that of CD44 caused diminished tethering, but no change in surface distribution indicating that both microvillus positioning and cytoskeletal anchoring contribute to leukocyte tethering. These findings demonstrate that TM domains of L-selectin and CD44 play a crucial role in cell adhesion under flow by targeting receptors to microvilli or the cell body, respectively.

6 Zusammenfassung

Das angeborene und erworbene Immunsystem umfasst verschiedene Zelltypen, die zur Ausübung ihrer Funktion die Blutbahn in Richtung Gewebe verlassen müssen. Zur Kommunikation der Zellen mit dem Gefäßendothel dienen Oberflächenrezeptoren, deren sequentieller Einsatz zur Extravasation führt. In Lymphozyten ist der initiale Schritt abhängig von L-Selektin (CD62L). Es ist bekannt, dass lymphozytäres L-Selektin fast ausschliesslich auf membranären Protrusionen, den Mikrovilli, exprimiert ist während der planare Zellkörper weitgehend ausgespart bleibt. Auch eine Vielzahl anderer Membranproteine werden aktiv in diesen Mikrodomänen gruppiert. Da diese besondere Oberflächentopologie eine funktionelle Bedeutung für die zelluläre Adhäsionsrate hat, ist die Entschlüsselung der biochemischen Mechanismen, die an der Kompartmentalisierung von Rezeptoren auf der Zelloberfläche beteiligt sind, von hoher Bedeutung.

In der vorliegenden Arbeit wurde der Einfluß der extrazellulären (EC), transmembranären (TM) und intrazellulären (IC) Domäne von CD44, einem Protein mit Lokalisierung ausschliesslich auf dem planaren Zellkörper, und L-Selektin auf die Zelloberflächentopologie beider Proteine untersucht. Für diese Untersuchungen wurden chimäre Formen beider Adhäsionsrezeptoren konstruiert, in denen eine oder mehrere Domänen gezielt ausgetauscht wurden. Die chimären Proteine wurden in einem Modellsystem mit humanen K562 Zellen exprimiert und die Rezeptortopologie mittels Elektronenmikroskopie qualitativ und quantitiv ausgewertet. Mittels Flusskammerexperimenten konnte anschliessend die funktionelle Bedeutung der Oberflächenlokalisation beider Adhäsionsproteine eruiert werden.

Es zeigte sich, daß die TM Domäne alleine die Lokalisation des Rezeptors auf der Zelloberfläche bestimmt. Der TM Abschnitt von CD44 führte unabhängig von der IC und EC Komponente zur Expression auf dem Zellkörper mit Aussparung der Mikrovilli. Entsprechend bewirkte der TM Abschnitt von L-Selektin eine ausschliesslich mikrovilläre Lokalisation. Die IC Verankerung von L-Selektin oder CD44 hatte keinen spezifischen Einfluß. Funktionell zeigten mikrovillär

exprimierte Rezeptoren eine höhere Adhäsionsrate unter Fluss, aber nicht unter statischen Bedingungen. Wurde in CD44 die TM Domöne durch die von L-Selektin ersetzt, führte dies zu einer deutlichen Steigerung der Adhäsionsfähigkeit der transfizierten Zellen auf Hyaluronsäure unter Fluss-bedingungen. Austausch der IC Domäne von L-Selektin durch die von CD44 führte zu geringerer Adhäsion trotz gleichbleibender Membranpositionierung, was die Bedeutung der Verankerung von L-Selektin an das Zytoskelett für seine Funktionalität unterstreicht.

Insgesamt zeigt diese Arbeit einen neuen Mechanismus der Kompart-mentalisierung von Oberflächenrezeptoren in unpolarisierten Zellen, der alleine durch transmembranäre Signale gesteuert wird und relevante Auswirkungen auf die zelluläre Adhäsion von Zellen des Immunsystems hat.

7 Abbreviations

- aa Amino Acid
- BSA Bovine Serum Albumin
- bp Base pairs
- CB Cell Body
- CCC CD44 wildtype, human
- CCL CD44 EC and TM domain linked to L-selectin IC domain
- CLC CD44 with substituted TM domain
- CLL CD44 EC domain linked to L-selectin TM and IC domain
- CCR Chemokine Receptor
- CD Cluster of Differentiation
- CMV Cytomegalovirus
- COPD Chronic Obstructive Pulmonary Disease
- CXCR Chemokine Receptor (CXC motif)
- dATP Deoxyadenosine Triphosphate
- dCTP Deoxycytidine Triphosphate
- dGTP Deoxyguanosine Triphosphate
- dNTP Deoxynucleoside Triphosphate
- dTTP Deoxythymidine Triphosphate
- DMSO Dimethyl Sulfoxide
- DNA Deoxyribonucleic Acid
- EC Extracellular
- EDTA Ethylenediaminetetraacetic acid
- EGF Epidermal Growth Factor
- EM Electron microscopy
- ERM Ezrin/Radixin/Moesin
- FDA US Food and Drug Administration
- FITC Fluorescein
- GlyCAM-1 Glycosylation-dependent Cell Adhesion Molecule 1
- HEPES 4-(2-hydroxyethyl)-1-piperazineethanesulfonic acid
- HEV High Endothelial Venules

- IC Intracellular
- ICAM-1 Intercellular Adhesion Molecule 1, CD54
- IgG Immunglobulin G
- kDa Kilo Dalton
- LAD Leukocyte Adhesion Deficiency Syndrome
- LB Luria-Bertani-Medium
- LCC L-selectin EC domain linked to CD44 TM and IC domain
- LCL L-selectin with substituted TM domain
- LFA-1 Lymphocyte function-associated antigen 1
- LLC L-selectin TM and EC domain linked to CD44 IC domain
- LLL L-selectin wildtype (CD62L), human
- mAb Monoclonal Antibody
- MAC-1 Macrophage-1 antigen, integrin $\alpha_M\beta_2$
- MAdCAM-1 Mucosal Addressin Cell Adhesion Molecule 1
- MFI Mean Fluorescence Intensity
- MV Microvillus
- PAGE Polyacrylamide Gel Electrophoresis
- PAMP Pathogen-associated Molecular Pattern
- PBS Phosphate Buffered Saline
- PCR Polymerase Chain Reaction
- PE Phycoerythrin
- PMN Polymorphonuclear cell, granulocyte
- PNAd Peripheral Node Addressins
- PSGL-1 P-selectin Glycoprotein Ligand 1
- RT Room temperature
- RT-PCR Reverse Transcriptase PCR
- SCR Short Consensus Repeat
- SD Standard Deviation
- SDS Sodium Dodecyl Sulfate
- sLex Sialyl Lewis X
- SOE Splicing by Overlap Extension
- TIRF Total internal reflection microscopy

- TM Transmembrane
- Tris Tris-hydroxymethylaminoethane
- Triton X T-octylphenoxypolyethoxyethanol
- Tween20 Polyoxyethylen(20)-sorbitan-monolaurat
- VCAM-1 Vascular Cell Adhesion Molecule 1, CD106
- VLA-4 Very late antigen-4, integrin $\alpha_1\beta_1$
- WBC White Blood Cell

8 References

1. Walter F. Boron. Medical Physiology, Updated Edition. Elsevier; 2004.
2. Ley, Tuma, Duran. Microcirculation, Handbook of Physiology. Elsevier; 2008.
3. Abbas AK, Lichtman AH, Pillai S. Cellular and Molecular Immunology. 6th ed. Saunders, Elsevier; 2007.
4. Fahraeus R. Die Strömungsverhältnisse und die Verteilung der Blutzellen im Gefäßsystem. Zur Frage der Bedeutung der intravaskulären Erythrozytenaggregation. Klin Wochenschr. 1928;7:100-106.
5. Fahraeus R. The suspension stability of the blood. Physiol Rev. 1929;9(9):241-274.
6. Fahraeus R, Lindqvist T. The viscosity of the blood in n arrow capillary tubes. Am J Physiol. 1931;96:562-568.
7. Schmid-Schönbein GW, Skalak R, Usami S, Chien S. Cell distribution in capillary networks. Microvascular Research. 1980 Jan;19(1):18-44.
8. Helmke BP, Bremner SN, Zweifach BW, Skalak R, Schmid-Schönbein GW. Mechanisms for increased blood flow resistance due to leukocytes. Am. J. Physiol. 1997 Dec;273(6 Pt 2):H2884-2890.
9. Schmid-Schönbein GW, Usami S, Skalak R, Chien S. The interaction of leukocytes and erythrocytes in capillary and postcapillary vessels. Microvasc. Res. 1980 Jan;19(1):45-70.
10. McKellar GE, McCarey DW, Sattar N, McInnes IB. Role for TNF in atherosclerosis? Lessons from autoimmune disease. Nat Rev Cardiol. 2009 Jun;6(6):410-417.
11. Khan F, Galarraga B, Belch JJF. The role of endothelial function and its assessment in rheumatoid arthritis. Nat Rev Rheumatol. 2010 May;6(5):253-261.
12. Medzhitov R. Origin and physiological roles of inflammation. Nature. 2008 Jul 24;454(7203):428-435.
13. Versari D, Daghini E, Virdis A, Ghiadoni L, Taddei S. Endothelial dysfunction as a target for prevention of cardiovascular disease. Diabetes Care. 2009 Nov;32 Suppl 2:S314-321.
14. Bakker W, Eringa EC, Sipkema P, van Hinsbergh VWM. Endothelial dysfunction and diabetes: roles of hyperglycemia, impaired insulin signaling and obesity. Cell Tissue Res. 2009 Jan;335(1):165-189.
15. van den Oever IAM, Raterman HG, Nurmohamed MT, Simsek S. Endothelial dysfunction, inflammation, and apoptosis in diabetes mellitus. Mediators Inflamm. 2010;2010:792393.
16. Rutkowski JM, Davis KE, Scherer PE. Mechanisms of obesity and related pathologies: the macro- and microcirculation of adipose tissue. FEBS J. 2009 Oct;276(20):5738-5746.
17. Wagner R. Erläuterungstafeln zur Physiologie und Entwicklungsgeschichte. Dresden: Leopold Voss; 1839.
18. Virchow R. Die Cellularpathologie in ihrer Begründung auf physiologische und pathologishe Gewebelehre. August Hirschwald Verlag; 1871.
19. Metchnikoff M. Lectures on the Comparative Pathology of Inflammation. Kegan Paul, Trench & Truebner & Co; 1893.
20. Springer TA. Traffic signals for lymphocyte recirculation and leukocyte emigration: the multistep paradigm. Cell. 1994 Jan 28;76(2):301-314.
21. Ley K, Laudanna C, Cybulsky MI, Nourshargh S. Getting to the site of inflammation: the leukocyte adhesion cascade updated. Nat. Rev. Immunol. 2007 Sep;7(9):678-689.
22. Ley K, Bullard DC, Arbonés ML, Bosse R, Vestweber D, Tedder TF, et al. Sequential contribution of L- and P-selectin to leukocyte rolling in vivo. J Exp Med. 1995 Feb 1;181(2):669-75.

23. Henderson RB, Lim LH, Tessier PA, Gavins FN, Mathies M, Perretti M, et al. The use of lymphocyte function-associated antigen (LFA)-1-deficient mice to determine the role of LFA-1, Mac-1, and alpha4 integrin in the inflammatory response of neutrophils. J. Exp. Med. 2001 Jul 16;194(2):219-226.

24. Reinhardt PH, Elliott JF, Kubes P. Neutrophils can adhere via alpha4beta1-integrin under flow conditions. Blood. 1997 May 15;89(10):3837-3846.

25. Alon R, Kassner PD, Carr MW, Finger EB, Hemler ME, Springer TA. The integrin VLA-4 supports tethering and rolling in flow on VCAM-1. J. Cell Biol. 1995 Mar;128(6):1243-1253.

26. Dunne JL, Ballantyne CM, Beaudet AL, Ley K. Control of leukocyte rolling velocity in TNF-alpha-induced inflammation by LFA-1 and Mac-1. Blood. 2002 Jan 1;99(1):336-341.

27. Campbell JJ, Hedrick J, Zlotnik A, Siani MA, Thompson DA, Butcher EC. Chemokines and the arrest of lymphocytes rolling under flow conditions. Science. 1998 Jan 16;279(5349):381-384.

28. Steeber DA, Campbell MA, Basit A, Ley K, Tedder TF. Optimal selectin-mediated rolling of leukocytes during inflammation in vivo requires intercellular adhesion molecule-1 expression. Proc. Natl. Acad. Sci. U.S.A. 1998 Jun 23;95(13):7562-7567.

29. Ley K. The role of selectins in inflammation and disease. Trends Mol Med. 2003 Jun;9(6):263-268.

30. Ley K, Kansas GS. Selectins in T-cell recruitment to non-lymphoid tissues and sites of inflammation. Nat. Rev. Immunol. 2004 May;4(5):325-335.

31. McEver RP. Misguided leukocyte adhesion. J. Clin. Invest. 1993 Jun;91(6):2340-2341.

32. McEver RP. Selectins. Curr. Opin. Immunol. 1994 Feb;6(1):75-84.

33. Bevilacqua MP, Stengelin S, Gimbrone MA, Seed B. Endothelial leukocyte adhesion molecule 1: an inducible receptor for neutrophils related to complement regulatory proteins and lectins. Science. 1989 Mar 3;243(4895):1160-1165.

34. Siegelman MH, van de Rijn M, Weissman IL. Mouse lymph node homing receptor cDNA clone encodes a glycoprotein revealing tandem interaction domains. Science. 1989 Mar 3;243(4895):1165-1172.

35. Kishimoto TK, Jutila MA, Berg EL, Butcher EC. Neutrophil Mac-1 and MEL-14 adhesion proteins inversely regulated by chemotactic factors. Science. 1989 Sep 15;245(4923):1238-1241.

36. Wedepohl S, Kaup M, Riese SB, Berger M, Dernedde J, Tauber R, et al. N-glycan analysis of recombinant L-Selectin reveals sulfated GalNAc and GalNAc-GalNAc motifs. J. Proteome Res. 2010 Jul 2;9(7):3403-3411.

37. Griffin JD, Spertini O, Ernst TJ, Belvin MP, Levine HB, Kanakura Y, et al. Granulocyte-macrophage colony-stimulating factor and other cytokines regulate surface expression of the leukocyte adhesion molecule-1 on human neutrophils, monocytes, and their precursors. J. Immunol. 1990 Jul 15;145(2):576-584.

38. Kishimoto TK, Jutila MA, Butcher EC. Identification of a human peripheral lymph node homing receptor: a rapidly down-regulated adhesion molecule. Proc. Natl. Acad. Sci. U.S.A. 1990 Mar;87(6):2244-2248.

39. Bruehl RE, Springer TA, Bainton DF. Quantitation of L-selectin distribution on human leukocyte microvilli by immunogold labeling and electron microscopy. J. Histochem. Cytochem. 1996 Aug;44(8):835-844.

40. Bargatze RF, Jutila MA, Butcher EC. Distinct roles of L-selectin and integrins alpha 4 beta 7 and LFA-1 in lymphocyte homing to Peyer's patch-HEV in situ: the multistep model confirmed and refined. Immunity. 1995 Jul;3(1):99-108.

41. Finger EB, Puri KD, Alon R, Lawrence MB, von Andrian UH, Springer TA. Adhesion through L-selectin requires a threshold hydrodynamic shear. Nature. 1996 Jan 18;379(6562):266-269.

42. Chen S, Springer TA. An automatic braking system that stabilizes leukocyte rolling by an increase in selectin bond number with shear. J. Cell Biol. 1999 Jan 11;144(1):185-200.

43. Marshall BT, Long M, Piper JW, Yago T, McEver RP, Zhu C. Direct observation of

catch bonds involving cell-adhesion molecules. Nature. 2003 May 8;423(6936):190-193.

44. Yago T, Wu J, Wey CD, Klopocki AG, Zhu C, McEver RP. Catch bonds govern adhesion through L-selectin at threshold shear. J. Cell Biol. 2004 Sep 13;166(6):913-923.

45. Lou J, Yago T, Klopocki AG, Mehta P, Chen W, Zarnitsyna VI, et al. Flow-enhanced adhesion regulated by a selectin interdomain hinge. J Cell Biol. 2006 Sep 25;174(7):1107-17.

46. Sako D, Comess KM, Barone KM, Camphausen RT, Cumming DA, Shaw GD. A sulfated peptide segment at the amino terminus of PSGL-1 is critical for P-selectin binding. Cell. 1995 Oct 20;83(2):323-331.

47. Cummings RD. Structure and function of the selectin ligand PSGL-1. Braz. J. Med. Biol. Res. 1999 May;32(5):519-528.

48. Puri KD, Finger EB, Gaudernack G, Springer TA. Sialomucin CD34 is the major L-selectin ligand in human tonsil high endothelial venules. J. Cell Biol. 1995 Oct;131(1):261-270.

49. Imai Y, Lasky LA, Rosen SD. Sulphation requirement for GlyCAM-1, an endothelial ligand for L-selectin. Nature. 1993 Feb 11;361(6412):555-557.

50. Sassetti C, Tangemann K, Singer MS, Kershaw DB, Rosen SD. Identification of podocalyxin-like protein as a high endothelial venule ligand for L-selectin: parallels to CD34. J. Exp. Med. 1998 Jun 15;187(12):1965-1975.

51. Samulowitz U, Kuhn A, Brachtendorf G, Nawroth R, Braun A, Bankfalvi A, et al. Human endomucin: distribution pattern, expression on high endothelial venules, and decoration with the MECA-79 epitope. Am. J. Pathol. 2002 May;160(5):1669-1681.

52. Berg EL, McEvoy LM, Berlin C, Bargatze RF, Butcher EC. L-selectin-mediated lymphocyte rolling on MAdCAM-1. Nature. 1993 Dec 16;366(6456):695-698.

53. Harms G, Kraft R, Grelle G, Volz B, Dernedde J, Tauber R. Identification of nucleolin as a new L-selectin ligand. Biochem. J. 2001 Dec 15;360(Pt 3):531-538.

54. Alon R, Fuhlbrigge RC, Finger EB, Springer TA. Interactions through L-selectin between leukocytes and adherent leukocytes nucleate rolling adhesions on selectins and VCAM-1 in shear flow. J Cell Biol. 1996 Nov;135(3):849-65.

55. Kunkel EJ, Chomas JE, Ley K. Role of primary and secondary capture for leukocyte accumulation in vivo. Circ. Res. 1998 Jan 9;82(1):30-38.

56. Eriksson EE, Xie X, Werr J, Thoren P, Lindbom L. Importance of primary capture and L-selectin-dependent secondary capture in leukocyte accumulation in inflammation and atherosclerosis in vivo. J Exp Med. 2001 Jul 16;194(2):205-18.

57. Jutila MA, Rott L, Berg EL, Butcher EC. Function and regulation of the neutrophil MEL-14 antigen in vivo: comparison with LFA-1 and MAC-1. J. Immunol. 1989 Nov 15;143(10):3318-3324.

58. Arbonés ML, Ord DC, Ley K, Ratech H, Maynard-Curry C, Otten G, et al. Lymphocyte homing and leukocyte rolling and migration are impaired in L-selectin-deficient mice. Immunity. 1994 Jul;1(4):247-260.

59. Jung U, Ley K. Mice lacking two or all three selectins demonstrate overlapping and distinct functions for each selectin. J Immunol. 1999 Jun 1;162(11):6755-62.

60. Goodison S, Urquidi V, Tarin D. CD44 cell adhesion molecules. MP, Mol. Pathol. 1999 Aug;52(4):189-196.

61. Konstantopoulos K, Thomas SN. Cancer cells in transit: the vascular interactions of tumor cells. Annu Rev Biomed Eng. 2009;11:177-202.

62. Aruffo A, Stamenkovic I, Melnick M, Underhill CB, Seed B. CD44 is the principal cell surface receptor for hyaluronate. Cell. 1990 Jun 29;61(7):1303-1313.

63. Burdick MM, Chu JT, Godar S, Sackstein R. HCELL is the major E- and L-selectin ligand expressed on LS174T colon carcinoma cells. J. Biol. Chem. 2006 May 19;281(20):13899-13905.

64. Legg JW, Isacke CM. Identification and functional analysis of the ezrin-binding site in the hyaluronan receptor, CD44. Curr. Biol. 1998 Jun 4;8(12):705-708.

65. Siegelman MH, DeGrendele HC, Estess P. Activation and interaction of CD44 and hyaluronan in immunological systems. J. Leukoc. Biol. 1999 Aug;66(2):315-321.

66. DeGrendele HC, Estess P, Picker LJ, Siegelman MH. CD44 and its ligand hyaluronate mediate rolling under physiologic flow: a novel lymphocyte-endothelial cell primary adhesion pathway. J. Exp. Med. 1996 Mar 1;183(3):1119-1130.

67. Vermeulen M, Le Pesteur F, Gagnerault MC, Mary JY, Sainteny F, Lepault F. Role of adhesion molecules in the homing and mobilization of murine hematopoietic stem and progenitor cells. Blood. 1998 Aug 1;92(3):894-900.

68. Dow LE, Humbert PO. Polarity regulators and the control of epithelial architecture, cell migration, and tumorigenesis. Int. Rev. Cytol. 2007;262:253-302.

69. Chhabra ES, Higgs HN. The many faces of actin: matching assembly factors with cellular structures. Nat Cell Biol. 2007 Oct;9(10):1110-21.

70. Small JV, Stradal T, Vignal E, Rottner K. The lamellipodium: where motility begins. Trends Cell Biol. 2002 Mar;12(3):112-120.

71. Majstoravich S, Zhang J, Nicholson-Dykstra S, Linder S, Friedrich W, Siminovitch KA, et al. Lymphocyte microvilli are dynamic, actin-dependent structures that do not require Wiskott-Aldrich syndrome protein (WASp) for their morphology. Blood. 2004 Sep 1;104(5):1396-403.

72. Shao JY, Ting-Beall HP, Hochmuth RM. Static and dynamic lengths of neutrophil microvilli. Proc. Natl. Acad. Sci. U.S.A. 1998 Jun 9;95(12):6797-6802.

73. Gorelik J, Shevchuk AI, Frolenkov GI, Diakonov IA, Lab MJ, Kros CJ, et al. Dynamic assembly of surface structures in living cells. Proc. Natl. Acad. Sci. U.S.A. 2003 May 13;100(10):5819-5822.

74. Hao J-J, Wang G, Pisitkun T, Patino-Lopez G, Nagashima K, Knepper MA, et al. Enrichment of distinct microfilament-associated and GTP-binding-proteins in membrane/microvilli fractions from lymphoid cells. J Proteome Res. 2008 Jul;7(7):2911-27.

75. von Andrian UH, Hasslen SR, Nelson RD, Erlandsen SL, Butcher EC. A central role for microvillous receptor presentation in leukocyte adhesion under flow. Cell. 1995 Sep 22;82(6):989-999.

76. Berlin C, Bargatze RF, Campbell JJ, von Andrian UH, Szabo MC, Hasslen SR, et al. alpha 4 integrins mediate lymphocyte attachment and rolling under physiologic flow. Cell. 1995 Feb 10;80(3):413-22.

77. Miner JJ, Xia L, Yago T, Kappelmayer J, Liu Z, Klopocki AG, et al. Separable requirements for cytoplasmic domain of PSGL-1 in leukocyte rolling and signaling under flow. Blood. 2008 Sep 1;112(5):2035-2045.

78. Bruehl RE, Moore KL, Lorant DE, Borregaard N, Zimmerman GA, McEver RP, et al. Leukocyte activation induces surface redistribution of P-selectin glycoprotein ligand-1. J. Leukoc. Biol. 1997 Apr;61(4):489-499.

79. Singer II, Scott S, Kawka DW, Chin J, Daugherty BL, DeMartino JA, et al. CCR5, CXCR4, and CD4 are clustered and closely apposed on microvilli of human macrophages and T cells. J. Virol. 2001 Apr;75(8):3779-3790.

80. Abitorabi MA, Pachynski RK, Ferrando RE, Tidswell M, Erle DJ. Presentation of integrins on leukocyte microvilli: a role for the extracellular domain in determining membrane localization. J. Cell Biol. 1997 Oct 20;139(2):563-571.

81. Erlandsen SL, Hasslen SR, Nelson RD. Detection and spatial distribution of the beta 2 integrin (Mac-1) and L-selectin (LECAM-1) adherence receptors on human neutrophils by high-resolution field emission SEM. J. Histochem. Cytochem. 1993 Mar;41(3):327-333.

82. Hocdé SA, Hyrien O, Waugh RE. Cell adhesion molecule distribution relative to neutrophil surface topography assessed by TIRFM. Biophys. J. 2009 Jul 8;97(1):379-387.

83. Bonifacino JS, Traub LM. Signals for sorting of transmembrane proteins to endosomes and lysosomes. Annu. Rev. Biochem. 2003;72:395-447.

84. Ivetic A, Florey O, Deka J, Haskard DO, Ager A, Ridley AJ. Mutagenesis of the Ezrin-

Radixin-Moesin Binding Domain of L-selectin Tail Affects Shedding, Microvillar Positioning, and Leukocyte Tethering. J. Biol. Chem. 2004 Aug 6;279(32):33263-33272.

85. Pavalko FM, Walker DM, Graham L, Goheen M, Doerschuk CM, Kansas GS. The cytoplasmic domain of L-selectin interacts with cytoskeletal proteins via alpha-actinin: receptor positioning in microvilli does not require interaction with alpha-actinin. J. Cell Biol. 1995 May;129(4):1155-1164.

86. Stein JV, Cheng G, Stockton BM, Fors BP, Butcher EC, von Andrian UH. L-selectin-mediated leukocyte adhesion in vivo: microvillous distribution determines tethering efficiency, but not rolling velocity. J. Exp. Med. 1999 Jan 4;189(1):37-50.

87. Finger E, Bruehl R, Bainton D, Springer T. A differential role for cell shape in neutrophil tethering and rolling on endothelial selectins under flow. The Journal of Immunology. 1996 Dec 1;157(11):5085 -5096.

88. Caputo KE, Hammer DA. Effect of microvillus deformability on leukocyte adhesion explored using adhesive dynamics simulations. Biophys. J. 2005 Jul;89(1):187-200.

89. Dong C, Cao J, Struble EJ, Lipowsky HH. Mechanics of leukocyte deformation and adhesion to endothelium in shear flow. Ann Biomed Eng. 1999 Jun;27(3):298-312.

90. Etzioni A, Frydman M, Pollack S, Avidor I, Phillips ML, Paulson JC, et al. Brief report: recurrent severe infections caused by a novel leukocyte adhesion deficiency. N. Engl. J. Med. 1992 Dec 17;327(25):1789-1792.

91. von Andrian UH, Berger EM, Ramezani L, Chambers JD, Ochs HD, Harlan JM, et al. In vivo behavior of neutrophils from two patients with distinct inherited leukocyte adhesion deficiency syndromes. J. Clin. Invest. 1993 Jun;91(6):2893-2897.

92. Anderson DC, Springer TA. Leukocyte adhesion deficiency: an inherited defect in the Mac-1, LFA-1, and p150,95 glycoproteins. Annu. Rev. Med. 1987;38:175-194.

93. Etzioni A. Genetic etiologies of leukocyte adhesion defects. Curr. Opin. Immunol. 2009 Oct;21(5):481-486.

94. Dutt S, Ermann J, Tseng D, Liu YP, George TI, Fathman CG, et al. L-selectin and beta7 integrin on donor CD4 T cells are required for the early migration to host mesenteric lymph nodes and acute colitis of graft-versus-host disease. Blood. 2005 Dec 1;106(12):4009-4015.

95. Borsig L, Wong R, Hynes RO, Varki NM, Varki A. Synergistic effects of L- and P-selectin in facilitating tumor metastasis can involve non-mucin ligands and implicate leukocytes as enhancers of metastasis. Proc. Natl. Acad. Sci. U.S.A. 2002 Feb 19;99(4):2193-2198.

96. Laubli H, Stevenson JL, Varki A, Varki NM, Borsig L. L-Selectin Facilitation of Metastasis Involves Temporal Induction of Fut7-Dependent Ligands at Sites of Tumor Cell Arrest. Cancer Res. 2006 Feb 1;66(3):1536-1542.

97. Stevenson JL, Varki A, Borsig L. Heparin attenuates metastasis mainly due to inhibition of P- and L-selectin, but non-anticoagulant heparins can have additional effects. Thromb. Res. 2007;120 Suppl 2:S107-111.

98. Wahrenbrock M, Borsig L, Le D, Varki N, Varki A. Selectin-mucin interactions as a probable molecular explanation for the association of Trousseau syndrome with mucinous adenocarcinomas. J. Clin. Invest. 2003 Sep;112(6):853-862.

99. Azuma H, Takahara S, Ichimaru N, Wang JD, Itoh Y, Otsuki Y, et al. Marked prevention of tumor growth and metastasis by a novel immunosuppressive agent, FTY720, in mouse breast cancer models. Cancer Res. 2002 Mar 1;62(5):1410-1419.

100. Parkman R, Remold-O'Donnell E, Kenney DM, Perrine S, Rosen FS. Surface protein abnormalities in lymphocytes and platelets from patients with Wiskott-Aldrich syndrome. Lancet. 1981 Dec 19;2(8260-61):1387-1389.

101. Kenney D, Cairns L, Remold-O'Donnell E, Peterson J, Rosen FS, Parkman R. Morphological abnormalities in the lymphocytes of patients with the Wiskott-Aldrich syndrome. Blood. 1986 Dec;68(6):1329-1332.

102. Burns SO, Killock DJ, Moulding DA, Metelo J, Nunes J, Taylor RR, et al. A congenital activating mutant of WASp causes altered plasma membrane topography and adhesion

under flow in lymphocytes. Blood. 2010 Jul 1;115(26):5355-5365.

103. Fabene PF, Navarro Mora G, Martinello M, Rossi B, Merigo F, Ottoboni L, et al. A role for leukocyte-endothelial adhesion mechanisms in epilepsy. Nat. Med. 2008 Dec;14(12):1377-1383.

104. González-Amaro R, Mittelbrunn M, Sánchez-Madrid F. Therapeutic anti-integrin (alpha4 and alphaL) monoclonal antibodies: two-edged swords? Immunology. 2005 Nov;116(3):289-296.

105. Enders S, Bernhard G, Zakrzewicz A, Tauber R. Inhibition of L-selectin binding by polyacrylamide-based conjugates under defined flow conditions. Biochim. Biophys. Acta. 2007 Oct;1770(10):1441-1449.

106. Dernedde J, Rausch A, Weinhart M, Enders S, Tauber R, Licha K, et al. Dendritic polyglycerol sulfates as multivalent inhibitors of inflammation. Proc. Natl. Acad. Sci. U.S.A. 2010 Nov 16;107(46):19679-19684.

107. Rossi B, Constantin G. Anti-selectin therapy for the treatment of inflammatory diseases. Inflamm Allergy Drug Targets. 2008 Jun;7(2):85-93.

108. Aydt E, Wolff G. Development of synthetic pan-selectin antagonists: a new treatment strategy for chronic inflammation in asthma. Pathobiology. 2002 2003;70(5):297-301.

109. Shakibaei M, Zimmermann B, Scheller M. Endocytosis of integrin alpha 5 beta 1 (fibronectin receptor) of mouse peritoneal macrophages in vitro: an immunoelectron microscopic study. J. Struct. Biol. 1993 Dec;111(3):180-189.

110. Spertini O, Cordey AS, Monai N, Giuffrè L, Schapira M. P-selectin glycoprotein ligand 1 is a ligand for L-selectin on neutrophils, monocytes, and CD34+ hematopoietic progenitor cells. J. Cell Biol. 1996 Oct;135(2):523-531.

111. Puri KD, Finger EB, Springer TA. The faster kinetics of L-selectin than of E-selectin and P-selectin rolling at comparable binding strength. J. Immunol. 1997 Jan 1;158(1):405-413.

112. Sperandio M, Smith ML, Forlow SB, Olson TS, Xia L, McEver RP, et al. P-selectin glycoprotein ligand-1 mediates L-selectin-dependent leukocyte rolling in venules. J. Exp. Med. 2003 May 19;197(10):1355-1363.

113. Yonemura S, Hirao M, Doi Y, Takahashi N, Kondo T, Tsukita S, et al. Ezrin/radixin/moesin (ERM) proteins bind to a positively charged amino acid cluster in the juxta-membrane cytoplasmic domain of CD44, CD43, and ICAM-2. J. Cell Biol. 1998 Feb 23;140(4):885-895.

114. Tsukita S, Oishi K, Sato N, Sagara J, Kawai A, Tsukita S. ERM family members as molecular linkers between the cell surface glycoprotein CD44 and actin-based cytoskeletons. J. Cell Biol. 1994 Jul;126(2):391-401.

115. Matter K. Epithelial polarity: sorting out the sorters. Curr. Biol. 2000 Jan 13;10(1):R39-42.

116. Pieczynski J, Margolis B. Protein complexes that control renal epithelial polarity. Am. J. Physiol. Renal Physiol. 2011 Mar;300(3):F589-601.

117. Wang Q, Margolis B. Apical junctional complexes and cell polarity. Kidney Int. 2007 Dec;72(12):1448-1458.

118. Shin K, Fogg VC, Margolis B. Tight junctions and cell polarity. Annu. Rev. Cell Dev. Biol. 2006;22:207-235.

119. Hutagalung AH, Novick PJ. Role of Rab GTPases in membrane traffic and cell physiology. Physiol. Rev. 2011 Jan;91(1):119-149.

120. Matter K, Mellman I. Mechanisms of cell polarity: sorting and transport in epithelial cells. Curr. Opin. Cell Biol. 1994 Aug;6(4):545-554.

121. Foti M, Phelouzat M-A, Holm A, Rasmusson BJ, Carpentier J-L. p56Lck anchors CD4 to distinct microdomains on microvilli. Proc. Natl. Acad. Sci. U.S.A. 2002 Feb 19;99(4):2008-2013.

122. Brenner B, Gulbins E, Schlottmann K, Koppenhoefer U, Busch GL, Walzog B, et al. L-selectin activates the Ras pathway via the tyrosine kinase p56lck. Proc. Natl. Acad. Sci. U.S.A. 1996 Dec 24;93(26):15376-15381.

123. Corbeil D, Röper K, Hannah MJ, Hellwig A, Huttner WB. Selective localization of the polytopic membrane protein prominin in

microvilli of epithelial cells - a combination of apical sorting and retention in plasma membrane protrusions. J. Cell. Sci. 1999 Apr;112 (Pt 7):1023-1033.

124. Perschl A, Lesley J, English N, Hyman R, Trowbridge I. Transmembrane domain of CD44 is required for its detergent insolubility in fibroblasts. J Cell Sci. 1995 Mar 1;108(3):1033-1041.

125. Dwir O, Grabovsky V, Pasvolsky R, Manevich E, Shamri R, Gutwein P, et al. Membranal cholesterol is not required for L-selectin adhesiveness in primary lymphocytes but controls a chemokine-induced destabilization of L-selectin rolling adhesions. J. Immunol. 2007 Jul 15;179(2):1030-1038.

126. Röper K, Corbeil D, Huttner WB. Retention of prominin in microvilli reveals distinct cholesterol-based lipid micro-domains in the apical plasma membrane. Nat. Cell Biol. 2000 Sep;2(9):582-592.

127. Snapp KR, Craig R, Herron M, Nelson RD, Stoolman LM, Kansas GS. Dimerization of P-selectin glycoprotein ligand-1 (PSGL-1) required for optimal recognition of P-selectin. J. Cell Biol. 1998 Jul 13;142(1):263-270.

128. Kansas GS, Ley K, Munro JM, Tedder TF. Regulation of leukocyte rolling and adhesion to high endothelial venules through the cytoplasmic domain of L-selectin. J. Exp. Med. 1993 Mar 1;177(3):833-838.

129. Perschl A, Lesley J, English N, Trowbridge I, Hyman R. Role of CD44 cytoplasmic domain in hyaluronan binding. Eur. J. Immunol. 1995 Feb;25(2):495-501.

130. Firrell JC, Lipowsky HH. Leukocyte margination and deformation in mesenteric venules of rat. Am. J. Physiol. 1989 Jun;256(6 Pt 2):H1667-1674.

131. Moore DT, Berger BW, DeGrado WF. Protein-protein interactions in the membrane: sequence, structural, and biological motifs. Structure. 2008 Jul;16(7):991-1001.

132. Call ME, Wucherpfennig KW. The T cell receptor: critical role of the membrane environment in receptor assembly and function. Annu. Rev. Immunol. 2005;23:101-125.

133. Call ME, Pyrdol J, Wiedmann M, Wucherpfennig KW. The organizing principle in the formation of the T cell receptor-CD3 complex. Cell. 2002 Dec 27;111(7):967-979.

134. Li X, Pérez L, Pan Z, Fan H. The transmembrane domain of TACE regulates protein ectodomain shedding. Cell Res. 2007 Dec;17(12):985-98.

135. Horton RM, Hunt HD, Ho SN, Pullen JK, Pease LR. Engineering hybrid genes without the use of restriction enzymes: gene splicing by overlap extension. Gene. 1989 Apr 15;77(1):61-68.

136. Bacabac RG, Smit TH, Cowin SC, Van Loon JJWA, Nieuwstadt FTM, Heethaar R, et al. Dynamic shear stress in parallel-plate flow chambers. J Biomech. 2005 Jan;38(1):159-167.

9 Publications

Manuscripts

- **Buscher K**, Riese S, Shakibaei M, Reich C, Dernedde J, Tauber R, Ley K
  The transmembrane domains of L-selectin and CD44 regulate receptor cell surface positioning and leukocyte adhesion under flow.
  J. Biol. Chem **285**, 13490-13497 (2010)
- Wedepohl S, Beceren-Braun F, Riese S, **Buscher K**, Enders S, Bernhard G, Kilian K, Blanchard V, Dernedde J, Tauber R.
  L-selectin – a dynamic regulator of leukocyte migration
  Eur J Cell Biol. (05/2011) [in print]

Conference Abstracts

- **Buscher K**, Riese SB, Shakibaei M, Dernedde J, Tauber R
  The Adhesion Receptor L-selectin: Microvillus positioning and Leukocyte Adhesion under Flow is Regulated by the Transmembrane Domain
  European Congress of Immunology (ECI) 09/2009, Berlin
- Riese S, **Buscher K**, Shakibaei M, Dernedde J, Ley K, Tauber R
  Receptor Topology of L-selectin and CD44 is Determined by the Transmembrane Domains
  From Protein Structure to Membrane Dynamics, 2-3 December 2010
- Wedepohl S, Beceren-Braun F, **Buscher K**, Riese S, Dernedde J, Tauber R
  Structure and Function of the Adhesion Receptor L-selectin
  Membrane and Modules, 10-13 December 2009

10 Curriculum vitae

Mein Lebenslauf wird aus datenschutzrechtlichen Gründen in der elektronischen Version meiner Arbeit nicht veröffentlicht.

11 Eidesstaatliche Erklärung

Ich, Konrad-Robert Buscher, erkläre, dass ich die vorgelegte Dissertation mit dem Thema „Microvillus Positioning of L-selectin and CD44 and its Impact on Leukocyte Adhesion“ selbst verfasst und keine anderen als die angegebenen Quellen und Hilfsmittel benutzt, ohne die (unzulässige) Hilfe Dritter verfasst und auch in Teilen keine Kopien anderer Arbeiten dargestellt habe.

Ort, Datum	Unterschrift